

UNDERSTANDING POST-TRAINING STRUCTURAL CHANGES IN LARGE LANGUAGE MODELS

Xinyu He

School of Automation
Southeast University, Nanjing, China
220242115@seu.edu.cn

Xianghui Cao

School of Automation
Southeast University, Nanjing, China
xhcao@seu.edu.cn

ABSTRACT

Post-training fundamentally alters the behavior of large language models (LLMs), yet its impact on the internal parameter space remains poorly understood. In this work, we conduct a systematic singular value decomposition (SVD) analysis of principal linear layers in pretrained LLMs, focusing on two widely adopted post-training methods: *instruction tuning* and *long-chain-of-thought (Long-CoT) distillation*. Our analysis reveals two consistent and unexpected structural changes: **(1) a near-uniform geometric scaling of singular values across layers**, which theoretically modulates attention scores; and **(2) highly consistent orthogonal transformations are applied to the left and right singular vectors of each matrix**. Disrupting this orthogonal consistency leads to catastrophic performance degradation. Based on these findings, we propose a simple yet effective framework that interprets post-training as a reparameterization of fixed subspaces in the pre-trained parameter space. Further experiments reveal that singular value scaling behaves as a secondary effect, analogous to a temperature adjustment, whereas the core functional transformation lies in the coordinated rotation of singular vectors. These results challenge the prevailing view of the parameter space in large models as a black box, uncovering the first clear regularities in how parameters evolve during training, and providing a new perspective for deeper investigation into model parameter changes.

1 INTRODUCTION

The remarkable success of large language models (LLMs) has been substantially facilitated by post-training techniques. With approaches such as instruction tuning (Ouyang et al., 2022; Zhang et al., 2024b; Peng et al., 2023), alignment training (Schulman et al., 2017; Li et al., 2023b; Rafailov et al., 2024; DeepSeek-AI et al., 2025) and knowledge distillation (Xu et al., 2024; Gu et al., 2024; McDonald et al., 2024; Yang et al., 2024), LLMs have become increasingly usable and better aligned with human intent (Guo et al., 2024; Cai et al., 2025; Feng et al., 2024). Recent research on post-training has predominantly centered on algorithmic innovations such as *Direct Preference Optimization* (DPO) (Rafailov et al., 2024), *Group Relative Policy Optimization* (GRPO) (DeepSeek-AI et al., 2025), and *Dynamic sAmpling Policy Optimization* (DAPO) (Yu et al., 2025) to enhance the reasoning capabilities of LLMs. Alternatively, *long-chain-of-thought (Long-CoT) distillation* offers a more straightforward and practiced approach, enabling smaller models to acquire reasoning ability by distilling long chains of thought from large RL-trained models (DeepSeek-AI et al., 2025).

However, despite the empirical success of post-training, its underlying impact on the internal structure of model parameters remains insufficiently understood. Although recent studies have investigated post-training mechanisms and uncovered some novel insights (Du et al., 2025; Marks & Tegmark, 2024; Jain et al., 2024; Lee et al., 2024; Panickssery et al., 2024; Stolfo et al., 2024; Katz & Belinkov, 2023; Yao et al., 2025), their studies remain indirect—relying primarily on hidden representations or behavioral observations rather than exploring fundamental structural changes. Transformations in parameter space, especially weight matrices, which we often treat as black boxes, have not been systematically examined. **The extent to which post-training reshapes the representational capacity of the parameter space remains an unresolved problem.**

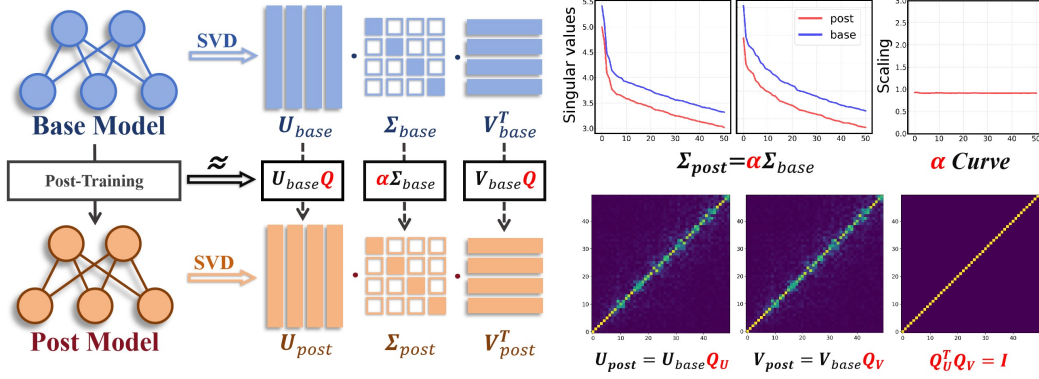


Figure 1: A simple but effective mathematical approximation to describe the effect of post-training on the parameter space. Performing SVD on weight matrices in the BASE model, post-training is equivalent to performing **linear scaling** on singular values and performing **consistent orthogonal transformations** on left and right singular vectors.

In this work, we present a systematic study on how post-training affects the parameter space of LLMs. Specifically, we focus on two token-level supervised post-training methods: **instruction tuning** and **Long-CoT distillation**¹. These methods underpin essential capabilities like instruction-following and reasoning, forming the basis for more advanced alignment techniques. To examine the structural impact of post-training, we analyze weight matrices using singular value decomposition (SVD). **SVD decomposes each matrix into orthogonal subspaces with distinct scaling factors, thereby reducing complex weight structures into three mathematically interpretable components for systematic analysis, making the underlying geometry of large model parameters more transparent and interpretable.** We apply this framework to the weight matrices within the Self-Attention modules and Feed-Forward Networks of publicly available models, and categorize models into three types: BASE models (e.g., *Qwen2.5-Math-1.5B* (Qwen et al., 2025)), INSTRUCT models (obtained through instruction tuning), and REASONING models (trained via long-CoT distillation, such as *DeepSeek R1-Distill-Qwen-1.5B* (DeepSeek-AI et al., 2025)). The latter two are collectively referred to as POST models. This categorization enables systematic comparison of parameter space structural changes induced by different post-training methods.

Our empirical results reveal two key effects of post-training on the model’s parameter space: **(1) Near-uniform geometric scaling of singular values:** Post-training preserves the principal singular value distribution of the BASE model while applying a consistent, layer-wise linear scaling factor. We show this scaling equivalently regulates attention scores. Notably, we observe anomalous scaling in the Attention module’s W_O matrix, which strongly correlates with the REASONING model’s superior long-chain reasoning over the INSTRUCT model; **(2) Highly consistent orthogonal transformations:** The left and right singular vectors of each matrix undergo nearly identical orthogonal transformations during post-training, exhibiting shared, coordinated rotations. This phenomenon occurs consistently across all weight matrices, strongly suggests that post-training preserves the subspaces structure established during pre-training.

These results indicate that post-training essentially induces highly regular structural perturbations in the parameter space. Based on the two observed phenomena, we can use a simple yet effective mathematical framework to directly approximate the impact of post-training on the parameter space (Figure 1). We experimentally demonstrate that the singular value scaling phenomenon is a temperature-controlled mechanism that does not alter the model’s behavior. The consistent orthogonal transformations applied to the weight matrices are the core of post-training.

We summarize our contributions as follows:

- **To the best of our knowledge, this is the first systematic study of structural changes in LLMs before/after post-training across the entire parameter space.** Unlike prior works focusing on individual neuron activations or external behaviors, we comprehensively analyze the singular

¹For clarity and ease of reading, *post-training* hereafter refers to both *instruction tuning* and *Long-CoT distillation* in the following sections unless otherwise specified.

value structure of principal linear layers, revealing consistent patterns of post-training effects in the parameter space.

- **We experimentally discover two structural phenomena that are stable across multiple model families, parameter sizes, and training methods:** First, the singular values exhibit near-uniform geometric scaling; second, the left and right singular vectors of each matrix remain stable under consistent orthogonal transformations.
- **We establish a simple yet effective mathematical framework to describe the parameter change mechanism.** Our experiments have validated the importance of orthogonal transformations in post-training. This work provides new understanding of parameter evolution during post-training and lays the foundation for developing a unified theory of LLM parameter transformations.

2 RELATED WORK

Interpretability of post-training. With the growing success of post-training, researchers have increasingly sought to uncover its underlying mechanisms. Several studies have attempted to investigate the impact of post-training on LLMs by constructing task-specific or instruction-formatted datasets (Du et al., 2025; Marks & Tegmark, 2024; Jain et al., 2024; Lee et al., 2024; Panickssery et al., 2024; He et al., 2024). However, since these studies treat the models more as black boxes, they provide limited insights into the structural changes in model parameters induced by post-training. Parallel lines of research have attempted to explain the behavior of large language models by analyzing individual neurons or sparse activation patterns, uncovering phenomena such as entropy neurons and task-specific circuits (Stolfo et al., 2024; Katz & Belinkov, 2023; Yao et al., 2025; Gurnee et al., 2024; Tang et al., 2024; Chen et al., 2024; Yu & Ananiadou, 2024). While these studies offer valuable insights, their scope is inherently limited, as they are often based on earlier models such as *GPT-2* (Brown et al., 2020), reducing their relevance to contemporary architectures. Our analysis is data-agnostic, as we directly examine the full parameter space of the model rather than relying on input-output behavior. This perspective extends beyond previous studies that focus on individual neurons or isolated functional circuits, enabling a more global understanding of model structure.

Singular value decomposition in large language models. The optimal low-rank approximation property of SVD (Eckart & Young, 1936) has inspired a surge of SVD-based techniques for LLMs. Recent methods such as *PiSSA* (Meng et al., 2024), *SVFT* (Lingam et al., 2024) and *RaSA* (He et al., 2025) leverage dominant singular components to improve fine-tuning efficiency, while others employ SVD for quantization to reduce deployment costs (Li et al., 2024; Wang et al., 2024; Qinsi et al.; Li et al., 2023a; Yuan et al., 2023). Beyond its practical utility, SVD provides a principled framework for analyzing the structure of LLMs (Yang et al., 2023). For any weight matrix, reduced SVD produces a decomposition into two orthogonal matrices and a diagonal matrix, each of which carries a well-defined mathematical role: the orthogonal matrices span the input and output subspaces, defining bases in which the transformation operates, while the diagonal matrix applies directional scaling along these bases. In this view, the singular vectors determine how representations are aligned and projected, and the singular values quantify the relative importance of each direction. This decomposition reveals how LLMs transform information across layers, making SVD not only a tool for compression or fine-tuning, but also a window into the geometry of their internal computation. Our work leverages this perspective to investigate the structural organization of weights in LLMs.

3 PRELIMINARIES

This section reviews the training pipeline and architectural components of LLMs. Given a vocabulary \mathcal{V} , we define LLMs as $\mathcal{M} : \mathcal{T} \rightarrow \mathcal{P}$, where \mathcal{T} denotes the set of input token sequences $T_i = [t_1, t_2, \dots, t_n]_i \in \mathcal{T}$ and \mathcal{P} is the probability space over \mathcal{V} . After \mathcal{M} accepts sequences of input tokens T_i , a probability distribution $p_{\mathcal{M}} \in \mathcal{P}$ is output to predict the probability of the next token.

Training stages of LLMs. LLMs are typically trained following a two-stage paradigm. The first stage, known as pre-training, involves optimizing a BASE model $\mathcal{M}_{\text{base}}$ to predict the next token given previous context, based on a large-scale corpus drawn from a large-scale distribution of natural language texts (Radford et al., 2018; Sun et al., 2021; Yuan et al., 2022). The second stage, termed post-training, further fine-tunes the pretrained model to align its behavior with specific

objectives, such as following user instructions (Zhang et al., 2024b) or performing complex reasoning (DeepSeek-AI et al., 2025). Depending on the post-training objective, the adapted model is referred to as an INSTRUCT model $\mathcal{M}_{\text{Instruct}}$ or a REASONING model $\mathcal{M}_{\text{reasoning}}$. The two models under discussion are collectively referred to as POST models $\mathcal{M}_{\text{post}}$. The architectures of $\mathcal{M}_{\text{base}}$ and $\mathcal{M}_{\text{post}}$ are identical — all weight matrices share the same dimensionality, while the sole distinction lies in their respective parameterizations. In the main paper, $\mathcal{M}_{\text{base}}$ refers to *Qwen2.5-Math-1.5B*, $\mathcal{M}_{\text{Instruct}}$ to its instruction-tuned variant *Qwen2.5-Math-1.5B-Instruct*, and $\mathcal{M}_{\text{reasoning}}$ to the distilled *reasoning* model *DeepSeek-R1-Distill-Qwen-1.5B*. Let $\mathcal{M}_{\text{Instruct}}, \mathcal{M}_{\text{reasoning}} \subset \mathcal{M}_{\text{post}}$. Results for other models across different families and parameter scales are provided in the Appendix.

Architectural components of LLMs. We focus on decoder-only Transformer-based models, which constitute the foundation of state-of-the-art large language model systems (OpenAI et al., 2024; DeepSeek-AI et al., 2024a; Team et al., 2025). The Transformer architecture consists of two core components: the Self-Attention Module (SA) and the Feed-Forward Network (FFN) (Vaswani et al., 2023). Given an input hidden vector $h^T \in \mathbb{R}^{d_{\text{model}}}$, we consider the simplest form of attention calculation for concise illustration. The output of the SA is:

$$SA(h) = \text{softmax} \left(\frac{hW_Q \cdot [K_{\text{cache}}; hW_K]^T}{\sqrt{d}} \right) \cdot [V_{\text{cache}}; hW_V]W_O \quad (1)$$

where $W_Q, W_K, W_V, W_O \in \mathbb{R}^{d_{\text{model}} \times d_{\text{model}}}$ are learnable weight matrices, \sqrt{d} is the scaling factor in the attention map, K_{cache} and V_{cache} are the key and value caches respectively, and $[...; ...]$ denotes concatenation. While modern architectures such as *Qwen2.5* series adopt variants like GQA (Ainslie et al., 2023) to optimize attention computation, the core projection matrices remain integral to the design due to their role in defining the attention mechanism’s representational capacity. Given an input vector $z^T \in \mathbb{R}^{d_{\text{model}}}$, the output of the FFN, which employs the *SwiGLU* activation function (Shazeer, 2020), is:

$$FFN(z) = (\text{SwiGLU}(z \cdot W_{\text{gate}}) \odot (z \cdot W_{\text{up}})) \cdot W_{\text{down}} \quad (2)$$

where $W_{\text{down}}, W_{\text{gate}}, W_{\text{up}} \in \mathbb{R}^{d_{\text{model}} \times d_{\text{mlp}}}$ are learnable weight matrices. Notably, GQA and SwiGLU-based FFNs have become fundamental building blocks adopted across numerous commercial open-source LLMs, including *Qwen* (Qwen et al., 2025), *LLaMA* (Grattafiori et al., 2024), *Mistral* (Jiang et al., 2023), *Phi-4* (Abdin et al., 2024), *gpt-oss* (OpenAI et al., 2025), *Gemma* (Team et al., 2025) and others (GLM et al., 2024; Yang et al., 2025; DeepSeek-AI et al., 2024b). Since our work targets components common to mainstream architectures, their widespread adoption inherently ensures the generalizability and representativeness of our research focus. We specifically focus on the weight matrices in SAs and FFNs, which account for the majority of parameters in LLMs. Analyzing these linear layers further enables us to characterize the structure of the model’s parameter space.

4 THE STRUCTURAL CHANGES OF SINGULAR SPACE AFTER POST-TRAINING

This section formally presents two regular structural changes that occur in the singular space of LLMs after post-training. Assuming that $m \geq n$, the reduced SVD of a matrix $W \in \mathbb{R}^{m \times n}$ is given by $W = U\Sigma V^T$, where $U \in \mathbb{R}^{m \times n}$ and $V \in \mathbb{R}^{n \times n}$ are matrices with orthogonality whose columns correspond to the left and right singular vectors respectively. The diagonal matrix $\Sigma = \text{diag}(\sigma_1, \sigma_2, \dots, \sigma_n) \in \mathbb{R}^{n \times n}$ contains the singular values arranged in descending order.

4.1 NEAR-UNIFORM GEOMETRIC SCALING OF SINGULAR VALUES

We observe that post-training does not alter the overall singular value distribution established during pre-training in the BASE model, instead, It exhibits a near-uniform geometric scaling behavior, characterized by approximately consistent scaling factors across main singular values.

For the i -th Transformer block of \mathcal{M}_A and \mathcal{M}_B of the same architecture, we perform reduced SVD on weight matrix:

$$\begin{aligned} W_A^{(i)} &= U_A^{(i)} \cdot \text{diag}(\sigma_{A,1}^{(i)}, \sigma_{A,2}^{(i)}, \dots, \sigma_{A,n}^{(i)}) \cdot V_A^{(i)T} \\ W_B^{(i)} &= U_B^{(i)} \cdot \text{diag}(\sigma_{B,1}^{(i)}, \sigma_{B,2}^{(i)}, \dots, \sigma_{B,n}^{(i)}) \cdot V_B^{(i)T} \end{aligned} \quad (3)$$

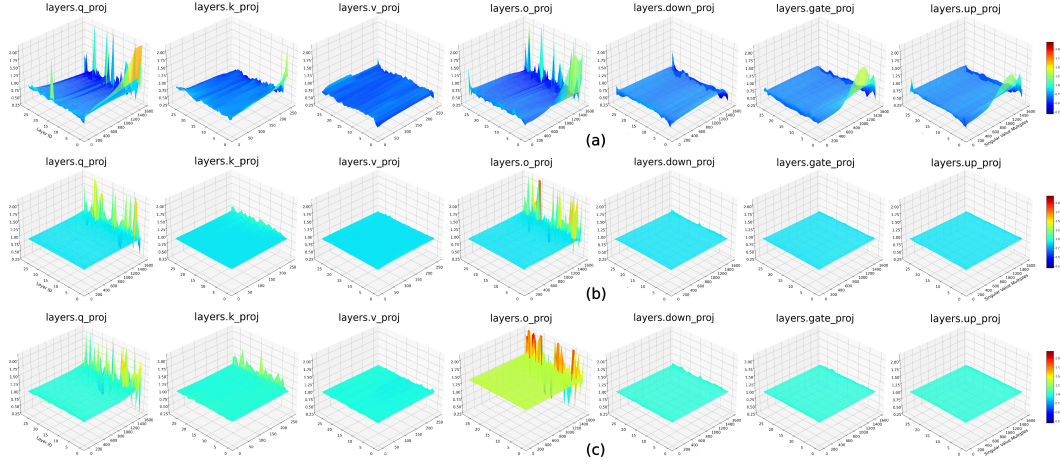


Figure 2: The heatmaps of SVSMs comparing $\mathcal{M}_{\text{base}}$ with $\mathcal{M}'_{\text{base}}$, $\mathcal{M}_{\text{Instruct}}$ and $\mathcal{M}_{\text{reasoning}}$. (a) indicates no regular pattern in the distribution of scaling factors between $\mathcal{M}'_{\text{base}}$ and $\mathcal{M}_{\text{base}}$. In both (b) and (c), the principal scaling exhibits a near-uniform distribution. While in (c), scaling factors of W_O are significantly higher than those of other matrix types.

where $W_A^{(i)} \in \mathcal{M}_A$ and $W_B^{(i)} \in \mathcal{M}_B$ represent weight matrices of the same type in the i -th Transformer block (e.g. W_Q) but belonging to different models. To quantify the effect of post-training on the evolution of singular value distribution, we define the *Singular Value Scaling Matrix* (SVSM) as:

$$SVSM(\frac{\mathcal{M}_B}{\mathcal{M}_A}) = [Div^{(1)}, Div^{(2)}, \dots, Div^{(k)}], \quad Div^{(i)} = [\frac{\sigma_{B,1}^{(i)}}{\sigma_{A,1}^{(i)}}, \dots, \frac{\sigma_{B,n}^{(i)}}{\sigma_{A,n}^{(i)}}]^T \quad (4)$$

where k corresponds to the depth of architecture \mathcal{M}_A or \mathcal{M}_B . $\alpha^{(i)} = \sigma_{B,j}^{(i)} / \sigma_{A,j}^{(i)}$, $j = 1, 2, \dots, n$ is the scaling factor. SVSM actually describes the distribution of all scaling factors across layers. We plot the heatmaps of $SVSM(\frac{\mathcal{M}_{\text{Instruct}}}{\mathcal{M}_{\text{base}}})$ (Figure 2b) and $SVSM(\frac{\mathcal{M}_{\text{reasoning}}}{\mathcal{M}_{\text{base}}})$ (Figure 2c) as examples. For reference comparison, we also show heatmaps of $SVSM(\frac{\mathcal{M}'_{\text{base}}}{\mathcal{M}_{\text{base}}})$ where $\mathcal{M}'_{\text{base}}$ denotes *Qwen2.5-1.5B*, which shares the same architecture but differs in pre-training data (Figure 2a).

For $\mathcal{M}_{\text{Instruct}}$ and $\mathcal{M}_{\text{reasoning}}$ compared to $\mathcal{M}_{\text{base}}$, scaling factors are remarkably stable across principal singular values. The instability is confined to the tail, where the singular values have negligible magnitude and contribute little to the overall transformation. This phenomenon can be approximately modeled by $\Sigma_{\text{post}} \approx \alpha \Sigma_{\text{base}}$ since the scaling factors of principal singular values are almost the same. As a comparison, the cross-layer stability cannot be achieved between $\mathcal{M}'_{\text{base}}$ and $\mathcal{M}_{\text{base}}$. We further observe that scaling factors of W_O in $\mathcal{M}_{\text{reasoning}}$ consistently exceed those of other matrix types, which can be used to significantly distinguish non-reasoning models. This pattern holds uniformly across all REASONING models in our study. Detailed quantitative data (Table 3) and visualizations of other models across different families and parameter scales are in Appendix A.

4.2 CONSISTENT ORTHOGONAL TRANSFORMATIONS OF SINGULAR VECTORS

We investigate the similarity between the singular vectors of BASE models and POST models. It is significant to find that the similarity matrices of both left and right singular vectors remain nearly identical after post-training, suggesting that the input and output subspaces undergo consistent orthogonal transformations during this process.

Combining Equation 3, the similarity matrices of $W_A^{(i)}$ and $W_B^{(i)}$ are defined as:

$$sim_U^{(i)}(\frac{\mathcal{M}_A}{\mathcal{M}_B}) = |U_A^{(i)T} \cdot U_B^{(i)}|, \quad sim_V^{(i)}(\frac{\mathcal{M}_A}{\mathcal{M}_B}) = |V_A^{(i)T} \cdot V_B^{(i)}| \quad (5)$$

where $|\cdot|$ takes the absolute value of each matrix element to remove the possible sign ambiguity of singular vectors. For $\mathcal{M}_{\text{base}} \rightarrow \mathcal{M}_{\text{post}}$, the change in left and right singular vectors from $W_{\text{base}}^{(i)}$ to

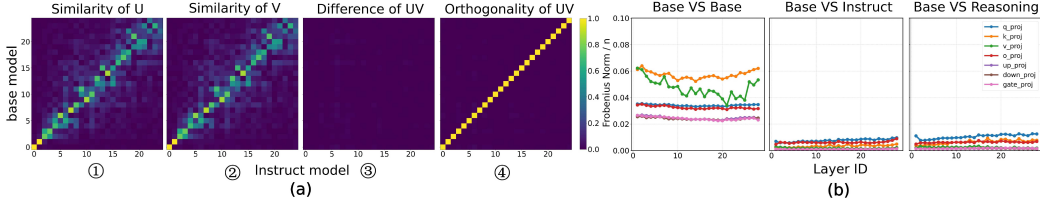


Figure 3: An example showing the orthogonality of singular vector similarity to the transformation performed. Only the first 25 dimensions are retained for clearer visualization. (a) show the singular vector behavior of W_O in the first Transformer block. Difference matrix (③) represents $|sim_U^{(0)} - sim_V^{(0)}|$, which is almost a zero matrix. ④ is $I_{orth}^{(0)}$ of $W_O^{(0)}$. Most of its diagonal elements are closed to 1, and the rest are basically 0. (b) extensively verifies the approximate equality of $Q_1^{(i)}$ and $Q_2^{(i)}$ comparing \mathcal{M}_{base} to \mathcal{M}'_{base} and \mathcal{M}_{post} .

$W_{post}^{(i)}$ is equivalent to applying orthogonal transformations to them:

$$U_{post}^{(i)} = U_{base}^{(i)} Q_1^{(i)}, \quad V_{post}^{(i)} = V_{base}^{(i)} Q_2^{(i)} \quad (6)$$

where $Q_1^{(i)}$ and $Q_2^{(i)}$ are orthogonal matrices (proof in Appendix G.2). Substituting Equation 6 into 5, we have $sim_U^{(i)}(\frac{\mathcal{M}_{base}}{\mathcal{M}_{post}}) = |Q_1^{(i)}|$ and $sim_V^{(i)}(\frac{\mathcal{M}_{base}}{\mathcal{M}_{post}}) = |Q_2^{(i)}|$, which indicates that the similarity matrix between singular vectors also represents their orthogonal transformations.

The widely observed phenomenon can be expressed as $sim_U^{(i)}(\frac{\mathcal{M}_{base}}{\mathcal{M}_{post}}) \approx sim_V^{(i)}(\frac{\mathcal{M}_{base}}{\mathcal{M}_{post}})$ (①-③ in Figure 3a), suggesting that $Q_1^{(i)}$ and $Q_2^{(i)}$ may exhibit a consistent underlying structure, with approximate equality representing a canonical case of this relationship. We verify it by utilizing the properties of orthogonal matrices:

$$if \ Q_1^{(i)} \approx Q_2^{(i)}, \ then \ Q_1^{(i)T} Q_2^{(i)} = (U_{base}^{(i)T} U_{post}^{(i)})^T \cdot (V_{base}^{(i)T} V_{post}^{(i)}) = I_{orth}^{(i)} \approx I \quad (7)$$

where $I \in \mathbb{R}^{n \times n}$ is the identity matrix. We quantify the equality between $Q_1^{(i)}$ and $Q_2^{(i)}$ by measuring the proximity of $I_{orth}^{(i)}$ to I , employing the normalized Frobenius norm $\mathcal{NF}^{(i)} = \mathcal{F}^{(i)}(I_{orth}^{(i)} - I) / \sqrt{n^2} = \mathcal{F}^{(i)}(I_{orth}^{(i)} - I) / n$ as our metric.

④ in Figure 3a presents our visualization of $I_{orth}^{(0)}$ for $W_O^{(0)}$, and Figure 3b illustrates $\mathcal{NF}^{(i)}$ in all the weight matrices of the layers. It can be observed that for \mathcal{M}_{post} , the values of $\mathcal{NF}^{(i)}$ are consistently and significantly lower than those of \mathcal{M}'_{base} across all layers, directly demonstrating that $Q_1^{(i)}$ and $Q_2^{(i)}$ are approximately equal orthogonal matrices throughout post-training. We can further conclude that the variation in singular vectors on the left and right can be approximately characterized by consistent orthogonal transformations with negligible deviation, a property absent in different pretrained models (see Appendix B.2). More detailed test results are in Appendix B.

5 ANALYSIS OF POST-TRAINING

The two observed phenomena enable a simplified mathematical model of the weight changes from $\mathcal{M}_{base} \rightarrow \mathcal{M}_{post}$, which prior work has struggled to describe formally (Du et al., 2025; Marks & Tegmark, 2024; Jain et al., 2024; Lee et al., 2024). For $W_{base} \in \mathcal{M}_{base}$ and $W_{post} \in \mathcal{M}_{post}$, the changes imposed by post-training on the parameters can be approximated by a linear factor α and an orthogonal matrix Q :

$$W_{post} = U_{post} \Sigma_{post} V_{post}^T \approx (U_{base} Q) \cdot (\alpha \Sigma_{base}) \cdot (V_{base} Q)^T \quad (8)$$

The relation $\Sigma_{post} = \alpha \Sigma_{base}$ captures how post-training globally scales the singular values, whereas $U_{post} = U_{base} Q$ and $V_{post} = V_{base} Q$ indicate a consistent orthogonal transformation of the input and output subspaces. From this perspective, post-training can be viewed as a reparameterization of the pretrained subspaces. This section provides empirical validation that post-training a BASE model fundamentally corresponds to learning structured orthogonal rotations, where singular value scaling constitutes a secondary effect.

5.1 SINGULAR VALUES SCALING IS JUST A TEMPERATURE-CONTROLLED MECHANISM

Equation 8 demonstrates that post-training does not alter the singular value distribution formed during pre-training in BASE models, but merely scales it proportionally. We designed a controlled experiment to verify the impact of post-training on the singular values of POST models.

Experiments. A direct corollary of Equation 8 is that the singular value distribution of POST models can be approximated by combining the singular value distribution of BASE models with an appropriate linear factor. Consequently, the models before and after singular value replacement should exhibit nearly identical performance. For $\mathcal{M}_{\text{post}}$, we perform Construction 9 on each of their weight matrices across all transformer blocks, which involves replacing the singular values of $\mathcal{M}_{\text{post}}$ with those from $\mathcal{M}_{\text{base}}$ and a given linear factor α' :

$$W_{\text{post}}^{(i)} \leftarrow U_{\text{post}}^{(i)} \cdot (\alpha' \Sigma_{\text{base}}^{(i)}) \cdot V_{\text{post}}^{(i)T} \quad (9)$$

We denote the resulting model after substitution of singular values as $\mathcal{M}_{\text{post}}^{\text{replaced}}$. The choice of α' is shown in Table 4. We then evaluate both $\mathcal{M}_{\text{post}}$ and $\mathcal{M}_{\text{post}}^{\text{replaced}}$ on four standard benchmarks: GSM8K (Cobbe et al., 2021), MATH-500 (Hendrycks et al., 2021b), MMLU (dev split) (Hendrycks et al., 2021a), and GPQA (Rein et al., 2023). Performance is measured by pass@1 accuracy(%) with a token limit of 1024. To ensure reliability, all evaluations are conducted with three independent repetitions, and the average values are reported. The results are shown in Table 1.

Table 1: Performance comparison between original and replaced models across GSM8K, MATH-500, MMLU, and GPQA with pass@1 accuracy(%).

BASE Models	REPLACED Types	GSM8K	MATH-500	MMLU (dev)	GPQA
<i>Qwen2.5-Math-1.5B</i>	$\mathcal{M}_{\text{Instruct}}$	85.14±0.14	65.47±0.90	48.04±0.60	30.44±0.36
	$\mathcal{M}_{\text{Instruct}}^{\text{replaced}}$	85.59±0.09	61.67±0.57	49.47±0.29	25.99±0.70
	$\mathcal{M}_{\text{reasoning}}$	62.88±0.59	32.73±1.64	25.02±0.59	7.02±0.44
	$\mathcal{M}_{\text{reasoning}}^{\text{replaced}}$	69.45±0.43	41.46±0.53	35.52±0.81	9.45±1.59

It can be observed that $\mathcal{M}_{\text{post}}^{\text{replaced}}$ maintains or even exceeds the performance of the $\mathcal{M}_{\text{post}}$, which once again illustrates the importance of Equation 8 and verifies that post-training does not alter the singular value distribution of the original model. Detailed experimental setups, the selection method of α' , and results across different model scales and families are provided in Appendix C.1.

Scaling of singular values is just a temperature-controlled mechanism. To better visualize the change mechanism of singular values, we directly employ Construction 14 (the equivalent expression of Construction 9 when all $\alpha' = 1$) to construct $\mathcal{M}_{\text{replaced}}$ and analyze the attention score distributions of the modified model (Figure 4a). The results show that the attention score distributions remain largely consistent, exhibiting no significant shifts. Instead, the replacement appears to induce a smoothing effect that resembles a temperature-controlled process (see Appendix G.1 for proof). The measure of *attention entropy* \mathcal{H} (Kumar & Sarawagi, 2019) in Figure 4b supports this potential mechanism. The attention entropy \mathcal{H} of $\mathcal{M}_{\text{replaced}}$ closely matches that of the original $\mathcal{M}_{\text{Instruct}}$, suggesting that the singular value replacement does not disrupt the structural integrity of LLMs or its capacity to capture contextual dependencies. More detailed results are given in Appendix C.2.

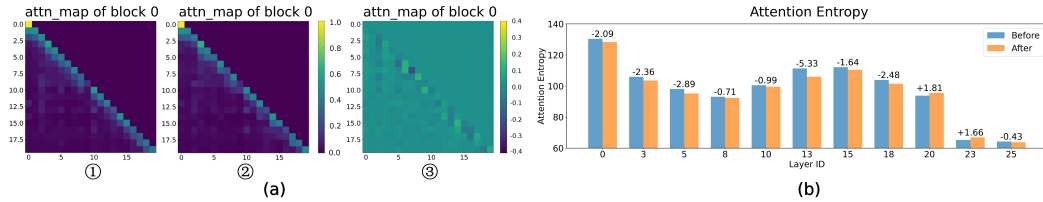


Figure 4: Visualization of the average attention patterns before and after replacing the singular values. ① in (a) shows the original attention heads, while ② presents the averaged attention heads from the modified model. ③ illustrates the differences between the original and modified attention patterns. Panel (b) suggests that this behavior corresponds to a modulation of attention entropy.

Notably, the attention entropy before and after the replacement remains closely aligned, suggesting that the entropy transformation induced by post-training primarily serves as a secondary temperature control mechanism rather than substantially altering the model’s behavior. This further implies that singular value scaling is a secondary effect accompanying the post-training process, not its primary mechanism.

5.2 CONSISTENT ORTHOGONAL TRANSFORMATIONS ARE THE CORE OF POST-TRAINING

While replacing the singular values only mildly alters the model’s behavior, disrupting the approximate orthogonal consistency between the input and output subspaces leads to a clear mode collapse in $\mathcal{M}_{\text{post}}$. To validate the functional importance of this coherence, we design a controlled experiment with two comparative settings.

Experiments. In the first setting (ABLATION), we remove the orthogonal transformation applied to the output subspaces of W_{post} (Construction 10), while preserving the transformation on the input subspaces. In the second setting (RESTORATION), we restore coherence by applying to the output subspaces the same orthogonal transformation derived from the input subspaces (Construction 11).

$$W_{\text{post}}^{(i)} \leftarrow U_{\text{post}}^{(i)} \Sigma_{\text{post}} \cdot V_{\text{base}}^{(i)T} \quad (10)$$

$$W_{\text{post}}^{(i)} \leftarrow U_{\text{post}}^{(i)} \Sigma_{\text{post}} \cdot (V_{\text{base}}^{(i)} Q)^T = U_{\text{post}}^{(i)} \Sigma_{\text{post}} \cdot (V_{\text{base}}^{(i)} \cdot U_{\text{base}}^{(i)T} U_{\text{post}}^{(i)T})^T \quad (11)$$

To assess the functional role of consistent orthogonal transformations, we feed the same input into $\mathcal{M}_{\text{post}}$ under three settings: the original model, the ABLATION model ($\mathcal{M}_{\text{post}}^{\text{ablation}}$), and the RESTORATION model ($\mathcal{M}_{\text{post}}^{\text{restoration}}$). All weight matrices in SAs are modified according to Constructions 10 and 11. We employ the same experimental setup as in Table 1 to evaluate the performance of restoration models across four datasets, with the results presented in Table 2:

Table 2: Performance comparison between original and RESTORATION models across GSM8K, MATH-500, MMLU, and GPQA with pass@1 accuracy(%).

BASE Models	RESTORATION Types	GSM8K	MATH-500	MMLU (dev)	GPQA
<i>Qwen2.5-Math-1.5B</i>	$\mathcal{M}_{\text{Instruct}}$	85.14±0.14	65.47±0.90	48.04±0.60	30.44±0.36
	$\mathcal{M}_{\text{Instruct}}^{\text{restoration}}$	84.53±0.25	66.20±0.16	41.28±0.44	27.69±0.29
	$\mathcal{M}_{\text{reasoning}}$	62.88±0.59	32.73±1.64	25.02±0.59	7.02±0.44
	$\mathcal{M}_{\text{reasoning}}^{\text{restoration}}$	61.54±1.19	30.93±0.57	29.00±0.44	6.75±0.27

We do not report the performance of ABLATION models because all of them produce **nonsensical outputs** across different tasks, as shown in the case examples in Figure 5, leading to 0% accuracy across all evaluation metrics. In contrast, RESTORATION models recover meaningful outputs, further supporting the hypothesis of consistent orthogonal transformations in LLMs. The results across different model scales and families are provided in the Appendix D.1.

QUESTION:

Janet’s ducks lay 16 eggs per day. She eats three for breakfast every morning and bakes muffins for her friends every day with four. She sells the remainder at the farmers’ market daily for \$2 per fresh duck egg. How much in dollars does she make every day at the farmers’ market?

Okay, so Janet has ducks that lay eggs, and she uses some for her own stuff. I need to ...
Thus, Janet makes **boxed{18}** dollars every day at the farmers’ market.

Original response ☒

putsHost former . organizers, td); J[t ; modeled,, . . Story . 详解 units PD Nap t through ther -f d fact through ~ ' . . Thing says put 着 . specific. . already . , lh , , l, through . / * . , explicit noth...

Ablation response ☐

Okay, let me try to figure out how much Janet makes every day at the farmers’ market. So, first ...
So, Janet makes ****boxed{18}**** every day at the farmers’ market.

Restoration response ☒

Figure 5: An example of model responses under three different settings. The ABLATION model outputs all garbled characters, while the RESTORATION model reconstructs the features of the original model through the orthogonal matrix of the input subspaces.

Orthogonal Consistency and Model Integrity. To further investigate the role of consistent orthogonal transformations in shaping the latent space across Transformer blocks, we evaluate the hidden

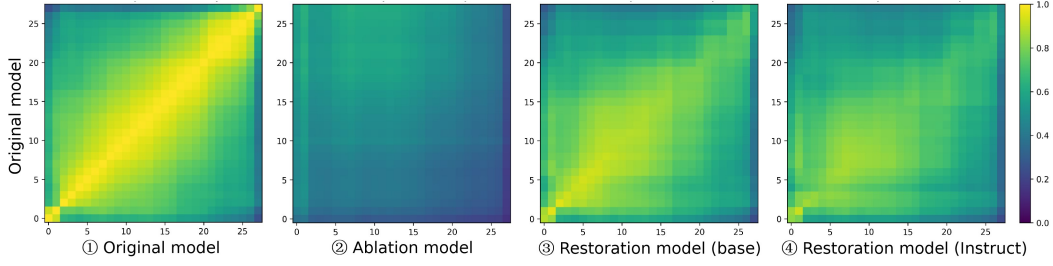


Figure 6: Heatmaps of CKA under different settings. ② corresponds to the ablation in Construction 10, which substantially disrupts the original model’s representational structure. ③ and ④, corresponding to restorations via Constructions 11 and 12, effectively recover the original hidden representations.

representations of the ABLATION and RESTORATION models using *Centered Kernel Alignment* (CKA) (Kornblith et al., 2019), a standard metric for quantifying representational similarity across neural network layers. We use 100 questions from the GSM8K dataset and compute the average hidden representation at each layer across these inputs. CKA scores are then calculated between the original model (①) and the ABLATION (②) and RESTORATION (③) models, as shown in Figure 6.

The results reveal that the ablation (②) leads to an immediate and significant disruption of the model’s representational structure starting from the very first layer. This indicates that the effect is not merely a result of cumulative downstream errors, but rather a fundamental alteration of the model’s initial architecture. The restoration process (③) effectively reinstates the original representational geometry, underscoring the structural importance of the orthogonal transformations.

Additional experimental settings and results are provided in Appendix D.2. These findings suggest that the consistent orthogonal transformations between the input and output subspaces represent a central mechanism driving parameter reorganization during post-training adaptation.

The equivalence of different post-training methods. We theoretically prove that POST models initialized from the same pretrained parameters but trained on different data distributions are mutually transformable via a shared set of orthogonal transformations (see Appendix G.3 for proof). To test this hypothesis, we construct a new RESTORATION model from $\mathcal{M}_{\text{Instruct}}$ following Construction 12, and evaluate its similarity to the original model using a CKA heatmap (marked as ④ in Figure 6). This effective restoration of the latent space confirms the correctness of the hypothesis.

$$W_{\text{post}}^{(i)} \leftarrow U_{\text{post}}^{(i)} \Sigma_{\text{post}} \cdot (V_{\text{Instruct}}^{(i)} Q')^T = U_{\text{post}}^{(i)} \Sigma_{\text{post}} \cdot (V_{\text{Instruct}}^{(i)} \cdot U_{\text{Instruct}}^{(i)}{}^T U_{\text{post}}^{(i)})^T \quad (12)$$

6 CONCLUSION

The paper establishes a unified and interpretable framework for understanding how post-training reshapes the internal structure of large language models. Through a comprehensive SVD analysis of linear layers, we identify two consistent transformations: a near-uniform geometric scaling of singular values and highly consistent orthogonal transformations of singular vectors, both pervasive across model families and parameter scales. Our theoretical and empirical analyses indicate that while singular value scaling can be interpreted as a temperature-like adjustment, the essential functional change lies in the structured rotations of singular vectors, whose disruption markedly degrades performance. These findings not only provide a theoretical foundation for potential applications (see Appendix F for a related discussion), but also offer the first systematic account of the reparameterization dynamics governing large language models.

7 LIMITATION

While this paper identifies two structural changes in the parameter space of SAs and FFNs, our analysis primarily focuses on weight matrices in models that undergo supervised post-training. This restriction naturally raises several open questions: **Do reinforcement learning–based post-training methods exhibit the same structural phenomena? If the architecture or training paradigm of large models changes substantially, will the observed regularities persist?** A detailed discussion in Appendix E further demonstrates the generality of these two structural changes.

Moreover, our findings also point to a deeper theoretical challenge: **what underlying mechanism gives rise to such striking regularities in LLMs?** We conjecture that a unified theoretical framework must exist—one capable of explaining the emergence and stability of these structural properties across different training paradigms. We view the pursuit of such a framework as a promising and impactful direction for future research.

REFERENCES

- Marah Abdin, Jyoti Aneja, Harkirat Behl, Sébastien Bubeck, Ronen Eldan, Suriya Gunasekar, et al. Phi-4 technical report, 2024. URL <https://arxiv.org/abs/2412.08905>.
- Joshua Ainslie, James Lee-Thorp, Michiel de Jong, Yury Zemlyanskiy, Federico Lebrón, and Sumit Sanghai. Gqa: Training generalized multi-query transformer models from multi-head checkpoints, 2023. URL <https://arxiv.org/abs/2305.13245>. <https://arxiv.org/abs/2305.13245>.
- Irwan Bello, Hieu Pham, Quoc V. Le, Mohammad Norouzi, and Samy Bengio. Neural combinatorial optimization with reinforcement learning, 2017. URL <https://arxiv.org/abs/1611.09940>.
- Iz Beltagy, Matthew E Peters, and Arman Cohan. Longformer: The long-document transformer. *arXiv preprint arXiv:2004.05150*, 2020.
- Tom B. Brown, Benjamin Mann, Nick Ryder, Melanie Subbiah, Jared Kaplan, Prafulla Dhariwal, Arvind Neelakantan, Pranav Shyam, Girish Sastry, Amanda Askell, Sandhini Agarwal, Ariel Herbert-Voss, et al. Language models are few-shot learners, 2020. URL <https://arxiv.org/abs/2005.14165>. <https://arxiv.org/abs/2005.14165>.
- Wenxiao Cai, Iaroslav Ponomarenko, Jianhao Yuan, Xiaoqi Li, Wankou Yang, Hao Dong, and Bo Zhao. Spatialbot: Precise spatial understanding with vision language models, 2025. URL <https://arxiv.org/abs/2406.13642>. <https://arxiv.org/abs/2406.13642>.
- Jianhui Chen, Xiaozhi Wang, Zijun Yao, Yushi Bai, Lei Hou, and Juanzi Li. Finding safety neurons in large language models. *arXiv preprint arXiv:2406.14144*, 2024.
- Shanbo Cheng, Yu Bao, Qian Cao, Luyang Huang, Liyan Kang, Zhicheng Liu, Yu Lu, Wenhao Zhu, Jingwen Chen, Zhichao Huang, Tao Li, Yifu Li, Huiying Lin, Sitong Liu, Ningxin Peng, Shuaijie She, Lu Xu, Nuo Xu, Sen Yang, Runsheng Yu, Yiming Yu, Liehao Zou, Hang Li, Lu Lu, Yuxuan Wang, and Yonghui Wu. Seed-x: Building strong multilingual translation llm with 7b parameters, 2025. URL <https://arxiv.org/abs/2507.13618>.
- Clément Christophe, Praveen K Kanithi, Tathagata Raha, Shadab Khan, and Marco AF Pimentel. Med42-v2: A suite of clinical llms, 2024. URL <https://arxiv.org/abs/2408.06142>.
- Tianzhe Chu, Yuexiang Zhai, Jihan Yang, Shengbang Tong, Saining Xie, Dale Schuurmans, Quoc V Le, Sergey Levine, and Yi Ma. Sft memorizes, rl generalizes: A comparative study of foundation model post-training. *arXiv preprint arXiv:2501.17161*, 2025.
- Karl Cobbe, Vineet Kosaraju, Mohammad Bavarian, Mark Chen, Heewoo Jun, Lukasz Kaiser, Matthias Plappert, Jerry Tworek, Jacob Hilton, Reiichiro Nakano, Christopher Hesse, and John Schulman. Training verifiers to solve math word problems, 2021. URL <https://arxiv.org/abs/2110.14168>. <https://arxiv.org/abs/2110.14168>.
- Jean-Philippe Corbeil, Amin Dada, Jean-Michel Attendu, Asma Ben Abacha, Alessandro Sordoni, Lucas Caccia, François Beaulieu, Thomas Lin, Jens Kleesiek, and Paul Vozila. A modular approach for clinical slms driven by synthetic data with pre-instruction tuning, model merging, and clinical-tasks alignment. *arXiv preprint arXiv:2505.10717*, 2025.
- DeepSeek-AI, Aixin Liu, Bei Feng, Bing Xue, Bingxuan Wang, Bochao Wu, Chengda Lu, Chenggang Zhao, Chengqi Deng, Chenyu Zhang, Chong Ruan, et al. Deepseek-v3 technical report, 2024a. <https://arxiv.org/abs/2412.19437>.

- DeepSeek-AI, Daya Guo, Dejian Yang, et al. Deepseek-rl: Incentivizing reasoning capability in llms via reinforcement learning, 2025. URL <https://arxiv.org/abs/2501.12948>. <https://arxiv.org/abs/2501.12948>.
- DeepSeek-AI et al. Deepseek llm: Scaling open-source language models with longtermism, 2024b. URL <https://arxiv.org/abs/2401.02954>.
- Hongzhe Du, Weikai Li, Min Cai, Karim Saraipour, Zimin Zhang, Himabindu Lakkaraju, Yizhou Sun, and Shichang Zhang. How post-training reshapes llms: A mechanistic view on knowledge, truthfulness, refusal, and confidence, 2025. URL <https://arxiv.org/abs/2504.02904>. <https://arxiv.org/abs/2504.02904>.
- Carl Eckart and Gale Young. The approximation of one matrix by another of lower rank. *Psychometrika*, 1(3):211–218, 1936.
- Xueyang Feng, Zhi-Yuan Chen, Yujia Qin, Yankai Lin, Xu Chen, Zhiyuan Liu, and Ji-Rong Wen. Large language model-based human-agent collaboration for complex task solving, 2024. URL <https://arxiv.org/abs/2402.12914>. <https://arxiv.org/abs/2402.12914>.
- Gemma Gemma Team, Morgane Riviere, Shreya Pathak, Pier Giuseppe Sessa, Cassidy Hardin, Surya Bhupatiraju, Léonard Hussenot, Thomas Mesnard, Bobak Shahriari, Alexandre Ramé, et al. Gemma 2: Improving open language models at a practical size. *arXiv preprint arXiv:2408.00118*, 2024.
- Team GLM, Aohan Zeng, Bin Xu, Bowen Wang, Chenhui Zhang, Da Yin, Dan Zhang, Diego Rojas, Guanyu Feng, et al. Chatglm: A family of large language models from glm-130b to glm-4 all tools, 2024. URL <https://arxiv.org/abs/2406.12793>.
- Aaron Grattafiori, Abhimanyu Dubey, Abhinav Jauhri, Abhinav Pandey, Abhishek Kadian, Ahmad Al-Dahle, Aiesha Letman, Akhil Mathur, Alan Schelten, Alex Vaughan, Amy Yang, Angela Fan, Anirudh Goyal, et al. The llama 3 herd of models, 2024. URL <https://arxiv.org/abs/2407.21783>. <https://arxiv.org/abs/2407.21783>.
- Yuxian Gu, Li Dong, Furu Wei, and Minlie Huang. Minillm: Knowledge distillation of large language models, 2024. URL <https://arxiv.org/abs/2306.08543>. <https://arxiv.org/abs/2306.08543>.
- Taicheng Guo, Xiuying Chen, Yaqi Wang, Ruidi Chang, Shichao Pei, Nitesh V. Chawla, Olaf Wiest, and Xiangliang Zhang. Large language model based multi-agents: A survey of progress and challenges, 2024. URL <https://arxiv.org/abs/2402.01680>. <https://arxiv.org/abs/2402.01680>.
- Wes Gurnee, Theo Horsley, Zifan Carl Guo, Tara Rezaei Kheirkhah, Qinyi Sun, Will Hathaway, Neel Nanda, and Dimitris Bertsimas. Universal neurons in gpt2 language models. *arXiv preprint arXiv:2401.12181*, 2024.
- Ashwin Kumar Gururajan, Enrique Lopez-Cuena, Jordi Bayarri-Planas, Adrian Tormos, Daniel Hinjos, Pablo Bernabeu-Perez, Anna Arias-Duart, Pablo Agustin Martin-Torres, Lucia Urcelay-Ganzabal, Marta Gonzalez-Mallo, Sergio Alvarez-Napagao, Eduard Ayguadé-Parra, and Ulises Cortés Dario Garcia-Gasulla. Aloe: A family of fine-tuned open healthcare llms, 2024. URL <https://arxiv.org/abs/2405.01886>.
- Tianyu He, Darshil Doshi, Aritra Das, and Andrey Gromov. Learning to grok: Emergence of in-context learning and skill composition in modular arithmetic tasks, 2024. URL <https://arxiv.org/abs/2406.02550>. <https://arxiv.org/abs/2406.02550>.
- Zhiwei He, Zhaopeng Tu, Xing Wang, Xingyu Chen, Zhijie Wang, Jiahao Xu, Tian Liang, Wenxiang Jiao, Zhuosheng Zhang, and Rui Wang. Rasa: Rank-sharing low-rank adaptation. *arXiv preprint arXiv:2503.12576*, 2025.
- Dan Hendrycks, Collin Burns, Steven Basart, Andy Zou, Mantas Mazeika, Dawn Song, and Jacob Steinhardt. Measuring massive multitask language understanding, 2021a. URL <https://arxiv.org/abs/2009.03300>. <https://arxiv.org/abs/2009.03300>.

- Dan Hendrycks, Collin Burns, Saurav Kadavath, Akul Arora, Steven Basart, Eric Tang, Dawn Song, and Jacob Steinhardt. Measuring mathematical problem solving with the math dataset, 2021b. URL <https://arxiv.org/abs/2103.03874>.
- Samyak Jain, Robert Kirk, Ekdeep Singh Lubana, Robert P. Dick, Hidenori Tanaka, Edward Grefenstette, Tim Rocktäschel, and David Scott Krueger. Mechanistically analyzing the effects of fine-tuning on procedurally defined tasks, 2024. URL <https://arxiv.org/abs/2311.12786>.
- Albert Q Jiang, Alexandre Sablayrolles, Arthur Mensch, Chris Bamford, Devendra Singh Chaplot, et al. Mistral 7b, 2023. URL <https://arxiv.org/abs/2310.06825>.
- Qiao Jin, Bhuwan Dhingra, Zhengping Liu, William W. Cohen, and Xinghua Lu. Pubmedqa: A dataset for biomedical research question answering, 2019. URL <https://arxiv.org/abs/1909.06146>.
- Shahar Katz and Yonatan Belinkov. Visit: Visualizing and interpreting the semantic information flow of transformers, 2023. URL <https://arxiv.org/abs/2305.13417>.
- Simon Kornblith, Mohammad Norouzi, Honglak Lee, and Geoffrey Hinton. Similarity of neural network representations revisited, 2019. URL <https://arxiv.org/abs/1905.00414>.
- Aviral Kumar and Sunita Sarawagi. Calibration of encoder decoder models for neural machine translation, 2019. URL <https://arxiv.org/abs/1903.00802>.
- Andrew Lee, Xiaoyan Bai, Itamar Pres, Martin Wattenberg, Jonathan K. Kummerfeld, and Rada Mihalcea. A mechanistic understanding of alignment algorithms: A case study on dpo and toxicity, 2024. URL <https://arxiv.org/abs/2401.01967>.
- Muyang Li, Yujun Lin, Zhekai Zhang, Tianle Cai, Xiuyu Li, Junxian Guo, Enze Xie, Chenlin Meng, Jun-Yan Zhu, and Song Han. Svdqunat: Absorbing outliers by low-rank components for 4-bit diffusion models. *arXiv preprint arXiv:2411.05007*, 2024.
- Yixiao Li, Yifan Yu, Chen Liang, Pengcheng He, Nikos Karampatziakis, Weizhu Chen, and Tuo Zhao. Loftq: Lora-fine-tuning-aware quantization for large language models. *arXiv preprint arXiv:2310.08659*, 2023a.
- Zihao Li, Zhuoran Yang, and Mengdi Wang. Reinforcement learning with human feedback: Learning dynamic choices via pessimism, 2023b. URL <https://arxiv.org/abs/2305.18438>.
- Vijay Chandra Lingam, Atula Neerkaje, Aditya Vavre, Aneesh Shetty, Gautham Krishna Gudur, Joydeep Ghosh, Eunsol Choi, Alex Dimakis, Aleksandar Bojchevski, and Sujay Sanghavi. Svft: Parameter-efficient fine-tuning with singular vectors. *Advances in Neural Information Processing Systems*, 37:41425–41446, 2024.
- Zihan Liu, Yang Chen, Mohammad Shoeybi, Bryan Catanzaro, and Wei Ping. Acemath: Advancing frontier math reasoning with post-training and reward modeling. *arXiv preprint*, 2024.
- Minh-Thang Luong, Hieu Pham, and Christopher D. Manning. Effective approaches to attention-based neural machine translation, 2015. URL <https://arxiv.org/abs/1508.04025>.
- Samuel Marks and Max Tegmark. The geometry of truth: Emergent linear structure in large language model representations of true/false datasets, 2024. URL <https://arxiv.org/abs/2310.06824>.
- Daniel McDonald, Rachael Papadopoulos, and Leslie Benningfield. Reducing llm hallucination using knowledge distillation: A case study with mistral large and mmlu benchmark. *Authorea Preprints*, 2024.

- Fanxu Meng, Zhaohui Wang, and Muhan Zhang. Pissa: Principal singular values and singular vectors adaptation of large language models. *Advances in Neural Information Processing Systems*, 37: 121038–121072, 2024.
- OpenAI, Aaron Hurst, et al. Gpt-4o system card, 2024. URL <https://arxiv.org/abs/2410.21276>. <https://arxiv.org/abs/2410.21276>.
- OpenAI, Sandhini Agarwal, Lama Ahmad, Jason Ai, Sam Altman, Andy Applebaum, et al. gpt-oss-120b & gpt-oss-20b model card, 2025. URL <https://arxiv.org/abs/2508.10925>.
- Long Ouyang, Jeff Wu, Xu Jiang, Diogo Almeida, Carroll L. Wainwright, Pamela Mishkin, Chong Zhang, Sandhini Agarwal, Katarina Slama, Alex Ray, John Schulman, Jacob Hilton, Fraser Kelton, Luke Miller, Maddie Simens, Amanda Askell, Peter Welinder, Paul Christiano, Jan Leike, and Ryan Lowe. Training language models to follow instructions with human feedback, 2022. URL <https://arxiv.org/abs/2203.02155>.
- Nina Panickssery, Nick Gabrieli, Julian Schulz, Meg Tong, Evan Hubinger, and Alexander Matt Turner. Steering llama 2 via contrastive activation addition, 2024. URL <https://arxiv.org/abs/2312.06681>. <https://arxiv.org/abs/2312.06681>.
- Baolin Peng, Chunyuan Li, Pengcheng He, Michel Galley, and Jianfeng Gao. Instruction tuning with gpt-4, 2023. URL <https://arxiv.org/abs/2304.03277>. [peng2023instructiontuninggpt4](https://arxiv.org/abs/2304.03277).
- Wang Qinsi, Jinghan Ke, Masayoshi Tomizuka, Kurt Keutzer, and Chenfeng Xu. Dobi-svd: Differentiable svd for llm compression and some new perspectives. In *The Thirteenth International Conference on Learning Representations*.
- Qwen, An Yang, Baosong Yang, Beichen Zhang, Binyuan Hui, Bo Zheng, Bowen Yu, et al. Qwen2.5 technical report, 2025. URL <https://arxiv.org/abs/2412.15115>. <https://arxiv.org/abs/2412.15115>.
- Alec Radford, Karthik Narasimhan, Tim Salimans, Ilya Sutskever, et al. Improving language understanding by generative pre-training. 2018.
- Rafael Rafailov, Archit Sharma, Eric Mitchell, Stefano Ermon, Christopher D. Manning, and Chelsea Finn. Direct preference optimization: Your language model is secretly a reward model, 2024. URL <https://arxiv.org/abs/2305.18290>. <https://arxiv.org/abs/2305.18290>.
- David Rein, Betty Li Hou, Asa Cooper Stickland, Jackson Petty, Richard Yuanzhe Pang, Julien Dirani, Julian Michael, and Samuel R. Bowman. Gpqa: A graduate-level google-proof q&a benchmark, 2023. URL <https://arxiv.org/abs/2311.12022>.
- John Schulman, Filip Wolski, Prafulla Dhariwal, Alec Radford, and Oleg Klimov. Proximal policy optimization algorithms, 2017. URL <https://arxiv.org/abs/1707.06347>. <https://arxiv.org/abs/1707.06347>.
- Zhihong Shao, Peiyi Wang, Qihao Zhu, Runxin Xu, Junxiao Song, Xiao Bi, Haowei Zhang, Mingchuan Zhang, YK Li, Yang Wu, et al. Deepseekmath: Pushing the limits of mathematical reasoning in open language models. *arXiv preprint arXiv:2402.03300*, 2024.
- Noam Shazeer. Glu variants improve transformer, 2020. URL <https://arxiv.org/abs/2002.05202>. <https://arxiv.org/abs/2002.05202>.
- Alessandro Stolfo, Ben Wu, Wes Gurnee, Yonatan Belinkov, Xingyi Song, Mrinmaya Sachan, and Neel Nanda. Confidence regulation neurons in language models, 2024. URL <https://arxiv.org/abs/2406.16254>. <https://arxiv.org/abs/2406.16254>.
- Yu Sun, Shuohuan Wang, Shikun Feng, Siyu Ding, Chao Pang, Junyuan Shang, Jiaxiang Liu, Xuyi Chen, Yanbin Zhao, Yuxiang Lu, et al. Ernie 3.0: Large-scale knowledge enhanced pre-training for language understanding and generation. *arXiv preprint arXiv:2107.02137*, 2021.

- Alon Talmor, Jonathan Herzig, Nicholas Lourie, and Jonathan Berant. Commonsenseqa: A question answering challenge targeting commonsense knowledge, 2019. URL <https://arxiv.org/abs/1811.00937>. <https://arxiv.org/abs/1811.00937>.
- Tianyi Tang, Wenyang Luo, Haoyang Huang, Dongdong Zhang, Xiaolei Wang, Xin Zhao, Furu Wei, and Ji-Rong Wen. Language-specific neurons: The key to multilingual capabilities in large language models. *arXiv preprint arXiv:2402.16438*, 2024.
- Gemma Team, Aishwarya Kamath, Johan Ferret, Shreya Pathak, Nino Vieillard, Ramona Merhej, Sarah Perrin, Tatiana Matejovicova, Alexandre Ramé, Morgane Rivière, Louis Rouillard, Thomas Mesnard, et al. Gemma 3 technical report, 2025. URL <https://arxiv.org/abs/2503.19786>. <https://arxiv.org/abs/2503.19786>.
- Ashish Vaswani, Noam Shazeer, Niki Parmar, Jakob Uszkoreit, Llion Jones, Aidan N. Gomez, Lukasz Kaiser, and Illia Polosukhin. Attention is all you need, 2023. URL <https://arxiv.org/abs/1706.03762>. <https://arxiv.org/abs/1706.03762>.
- Xin Wang, Yu Zheng, Zhongwei Wan, and Mi Zhang. Svd-llm: Truncation-aware singular value decomposition for large language model compression. *arXiv preprint arXiv:2403.07378*, 2024.
- Xiaohan Xu, Ming Li, Chongyang Tao, Tao Shen, Reynold Cheng, Jinyang Li, Can Xu, Dacheng Tao, and Tianyi Zhou. A survey on knowledge distillation of large language models, 2024. URL <https://arxiv.org/abs/2402.13116>. <https://arxiv.org/abs/2402.13116>.
- Aiyuan Yang et al. Baichuan 2: Open large-scale language models, 2025. URL <https://arxiv.org/abs/2309.10305>.
- Chuanpeng Yang, Yao Zhu, Wang Lu, Yidong Wang, Qian Chen, Chenlong Gao, Bingjie Yan, and Yiqiang Chen. Survey on knowledge distillation for large language models: methods, evaluation, and application. *ACM Transactions on Intelligent Systems and Technology*, 2024.
- Greg Yang, James B Simon, and Jeremy Bernstein. A spectral condition for feature learning. *arXiv preprint arXiv:2310.17813*, 2023.
- Yunzhi Yao, Ningyu Zhang, Zekun Xi, Mengru Wang, Ziwen Xu, Shumin Deng, and Huajun Chen. Knowledge circuits in pretrained transformers, 2025. URL <https://arxiv.org/abs/2405.17969>.
- Qiyang Yu, Zheng Zhang, Ruofei Zhu, Yufeng Yuan, Xiaochen Zuo, Yu Yue, Weinan Dai, Tiantian Fan, Gaohong Liu, Lingjun Liu, et al. Dapo: An open-source llm reinforcement learning system at scale. *arXiv preprint arXiv:2503.14476*, 2025.
- Zeping Yu and Sophia Ananiadou. Neuron-level knowledge attribution in large language models, 2024. URL <https://arxiv.org/abs/2312.12141>. <https://arxiv.org/abs/2312.12141>.
- Hongyi Yuan, Zheng Yuan, Ruyi Gan, Jiaying Zhang, Yutao Xie, and Sheng Yu. Biobart: Pretraining and evaluation of a biomedical generative language model. *arXiv preprint arXiv:2204.03905*, 2022.
- Zhihang Yuan, Yuzhang Shang, Yue Song, Qiang Wu, Yan Yan, and Guangyu Sun. Asvd: Activation-aware singular value decomposition for compressing large language models. *arXiv preprint arXiv:2312.05821*, 2023.
- Jie Zhang, Dongrui Liu, Chen Qian, Linfeng Zhang, Yong Liu, Yu Qiao, and Jing Shao. Reef: Representation encoding fingerprints for large language models. *arXiv preprint arXiv:2410.14273*, 2024a.
- Shengyu Zhang, Linfeng Dong, Xiaoya Li, Sen Zhang, Xiaofei Sun, Shuhe Wang, Jiwei Li, Runyi Hu, Tianwei Zhang, Fei Wu, and Guoyin Wang. Instruction tuning for large language models: A survey, 2024b. URL <https://arxiv.org/abs/2308.10792>. <https://arxiv.org/abs/2308.10792>.

A SINGULAR VALUE SCALING ACROSS MODELS OF DIFFERENT FAMILIES AND SIZES

In the main paper, we introduce the SVSMs of *Qwen2.5-Math-1.5B* as the BASE model. This section continues to present comparisons of models with different post-training methods based on BASE models *Qwen2.5-Math-7B*, *Llama-3.1-8B*, and *Qwen2.5-14B* in DeepSeek-AI et al. (2025). The different POST versions of these models are described in the Appendix H.2. We will also provide a detailed analysis of the cross-layer stability of the near-uniform geometric scaling.

A.1 SVSMs

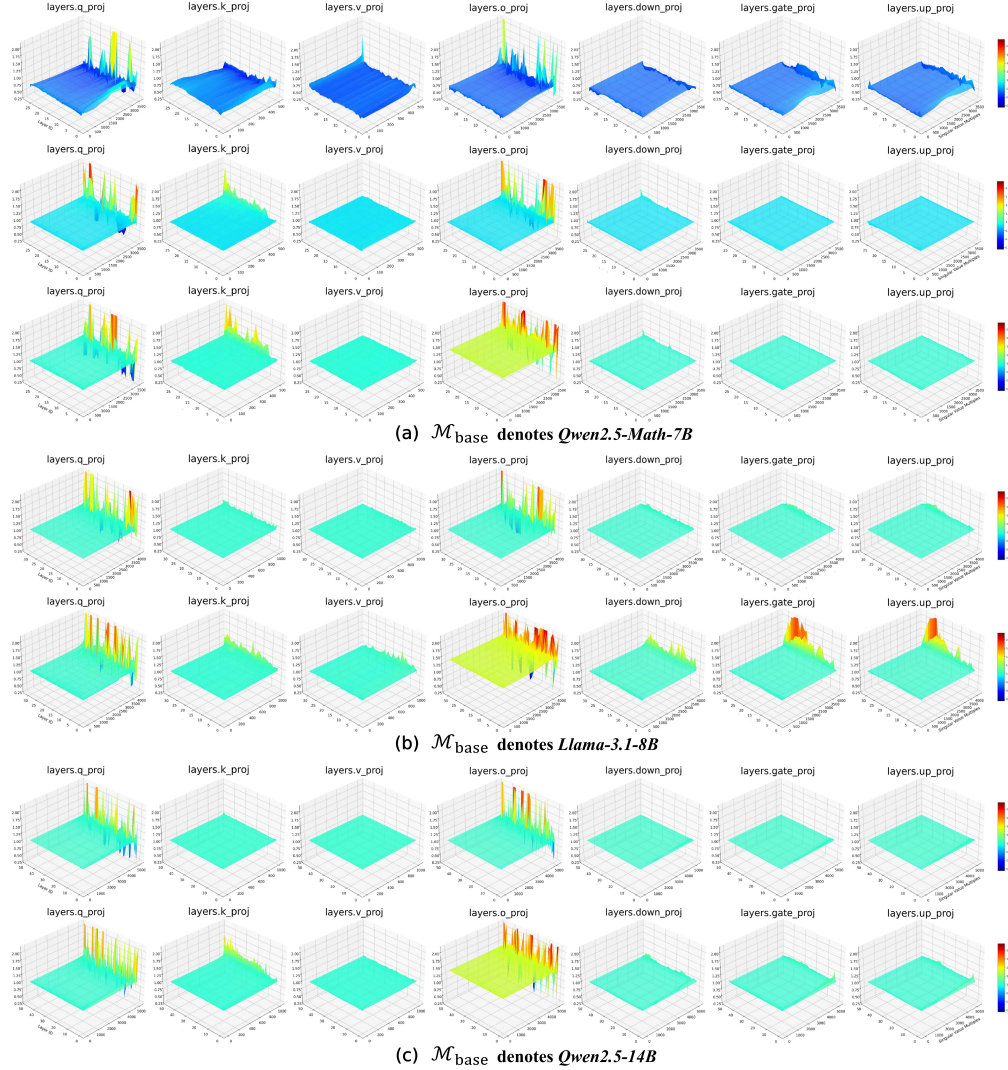


Figure 7: The heatmaps of SVSMs. The BASE models of (a), (b) and (c) are *Qwen2.5-Math-7B*, *Llama-3.1-8B* and *Qwen2.5-14B* respectively. Unlike *Qwen2.5-Math-7B* which has different pretrained versions like *Qwen2.5-7B*, only INSTRUCT version and REASONING version of the latter two models are compared.

Figure 7 shows SVSMs of different BASE models. We empirically observe a consistent pattern of singular value scaling across different post-training methods, where the principal singular values exhibit identical scaling ratios across different layers. This phenomenon universally manifests in all weight matrices. Notably, the W_O matrices in all REASONING models demonstrate significantly higher overall scaling ratios compared to other weight matrices.

A.2 CROSS-LAYER STABILITY OF SINGULAR VALUE SCALING

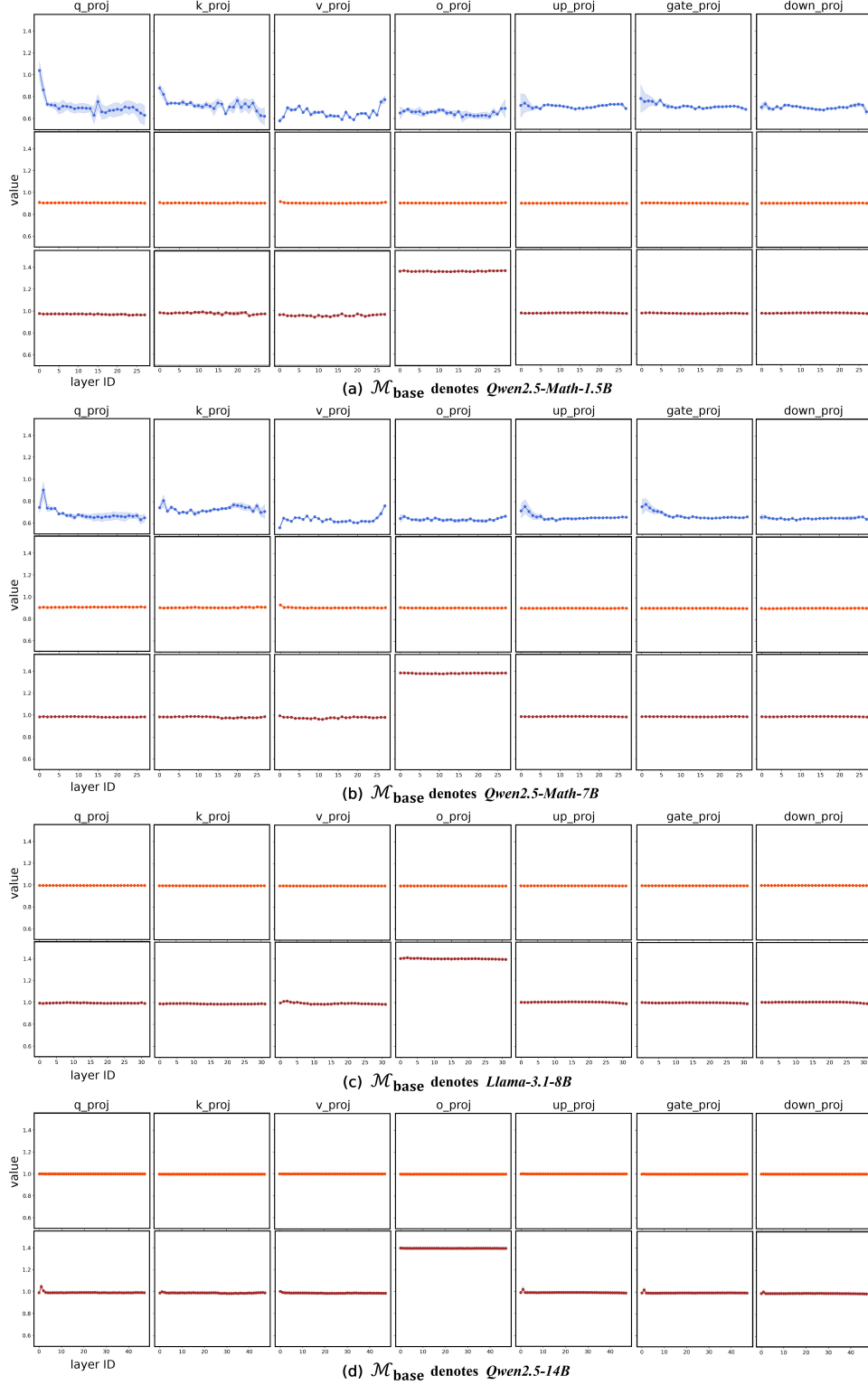


Figure 8: The bandwidth plot shows the distribution ($\text{mean} \pm \text{std}$) of the scaling factors for the top 90% singular values in each layer. The blue line indicates comparison with $\mathcal{M}'_{\text{base}}$, while the light orange and brown curves correspond to comparisons with $\mathcal{M}_{\text{instruct}}$ and $\mathcal{M}_{\text{reasoning}}$ respectively.

Figure 8 shows the mean (dark line) and standard deviation (light band) of the scaling factors for the top 90% principal singular values across all Transformer blocks. As can be seen from the figure, both the INSTRUCT and REASONING models show stability in singular value scaling, which is both per-layer (almost no broadband is visible in the INSTRUCT and REASONING models) and cross-layer (the values in each layer are almost the same). Table 3 further reports the overall mean and standard deviation of the scaling factors for the top 90% singular values across all layers. As shown, the standard deviation across different base models is substantially larger than that between each base model and its corresponding post model (e.g., 37.39 \times std for in *Qwen2.5-Math-1.5B* between $\mathcal{M}'_{\text{base}}$ and $\mathcal{M}_{\text{Instruct}}$), and the maximum variation of $\mathcal{M}_{\text{post}}$ remains within 1%, demonstrating the stability of the singular value scaling phenomenon and further reinforcing our claim.

Table 3: Global layer statistics of the scaling of the top 90% singular values ($mean \pm std$), measured for different model families and parameter scales.

	$SVSM(\frac{\cdot}{\mathcal{M}_{\text{base}}})$	W_Q	W_K	W_V	W_O
<i>Qwen2.5-Math-1.5B</i>	$\mathcal{M}'_{\text{base}}$	0.6709 ± 0.1728	0.7017 ± 0.0903	0.6465 ± 0.0432	0.6293 ± 0.1272
	$\mathcal{M}_{\text{Instruct}}$	0.9071 ± 0.0046	0.9084 ± 0.0053	0.9026 ± 0.0036	0.9041 ± 0.0036
	$\mathcal{M}_{\text{reasoning}}$	0.9710 ± 0.0131	0.9723 ± 0.0109	0.9513 ± 0.0103	1.3551 ± 0.0058
<i>Qwen2.5-Math-7B</i>	$\mathcal{M}'_{\text{base}}$	0.6621 ± 0.0827	0.7033 ± 0.0688	0.6388 ± 0.0368	0.6257 ± 0.0317
	$\mathcal{M}_{\text{Instruct}}$	0.9074 ± 0.0043	0.9103 ± 0.0111	0.9040 ± 0.0047	0.9056 ± 0.0027
	$\mathcal{M}_{\text{reasoning}}$	0.9837 ± 0.0036	0.9823 ± 0.0072	0.9737 ± 0.0072	1.3800 ± 0.0031
<i>Llama-3.1-8B</i>	$\mathcal{M}_{\text{Instruct}}$	0.9960 ± 0.0017	0.9951 ± 0.0008	0.9957 ± 0.0009	0.9975 ± 0.0027
	$\mathcal{M}_{\text{reasoning}}$	1.0041 ± 0.0181	0.9898 ± 0.0058	0.9930 ± 0.0093	1.4112 ± 0.0187
<i>Qwen2.5-14B</i>	$\mathcal{M}_{\text{Instruct}}$	0.9990 ± 0.0006	0.9989 ± 0.0003	0.9989 ± 0.0002	0.9989 ± 0.0002
	$\mathcal{M}_{\text{reasoning}}$	0.9937 ± 0.0142	0.9901 ± 0.0064	0.9861 ± 0.0031	1.3952 ± 0.0017

	$SVSM(\frac{\cdot}{\mathcal{M}_{\text{base}}})$	W_{up}	W_{gate}	W_{down}
<i>Qwen2.5-Math-1.5B</i>	$\mathcal{M}'_{\text{base}}$	0.7242 ± 0.0882	0.7282 ± 0.1179	0.6967 ± 0.0274
	$\mathcal{M}_{\text{Instruct}}$	0.9016 ± 0.0010	0.9018 ± 0.0017	0.9019 ± 0.0010
	$\mathcal{M}_{\text{reasoning}}$	0.9720 ± 0.0023	0.9687 ± 0.0035	0.9714 ± 0.0026
<i>Qwen2.5-Math-7B</i>	$\mathcal{M}'_{\text{base}}$	0.6693 ± 0.0454	0.6791 ± 0.0514	0.6495 ± 0.0140
	$\mathcal{M}_{\text{Instruct}}$	0.9021 ± 0.0014	0.9025 ± 0.0013	0.9024 ± 0.0016
	$\mathcal{M}_{\text{reasoning}}$	0.9847 ± 0.0020	0.9839 ± 0.0019	0.9843 ± 0.0021
<i>Llama-3.1-8B</i>	$\mathcal{M}_{\text{Instruct}}$	0.9961 ± 0.0003	0.9957 ± 0.0003	0.9961 ± 0.0003
	$\mathcal{M}_{\text{reasoning}}$	1.0036 ± 0.0041	0.9988 ± 0.0033	1.0035 ± 0.0044
<i>Qwen2.5-14B</i>	$\mathcal{M}_{\text{Instruct}}$	0.9991 ± 0.0021	0.9991 ± 0.0015	0.9990 ± 0.0006
	$\mathcal{M}_{\text{reasoning}}$	0.9922 ± 0.0132	0.9924 ± 0.0119	0.9909 ± 0.0062

B CONSISTENT ORTHOGONAL TRANSFORMATIONS ACROSS MODELS OF DIFFERENT FAMILIES AND SIZES

In this section, we compare $\mathcal{NF}^{(i)}$ between the BASE and POST versions of *Qwen2.5-Math-7B*, *Llama-3.1-8B*, and *Qwen2.5-14B*. We also visualize the similarity, difference, and orthogonality matrices of the left and right singular vectors of W_Q , W_K , W_V , and W_O (using the first and last Transformer blocks as examples), and discuss whether such orthogonal consistency is already present in the pre-training stage.

B.1 VISUALIZING ORTHOGONAL CONSISTENCY ACROSS MODELS OF DIFFERENT FAMILIES AND SIZES

As shown in Figure 9, the $\mathcal{NF}^{(i)}$ values across different POST versions consistently remain low, in contrast to the higher values observed among the pre-training variants (Figure 9a, *Base vs Base*). This indicates that, despite variations in model scale and post-training methods, each matrix exhibits a high degree of consistency in the orthogonal transformations ($Q_1^{(i)}$ and $Q_2^{(i)}$) applied to its singular vectors. This phenomenon is illustrated more clearly in Figure 10-13, where most orthogonality matrices closely approximate the identity matrix.

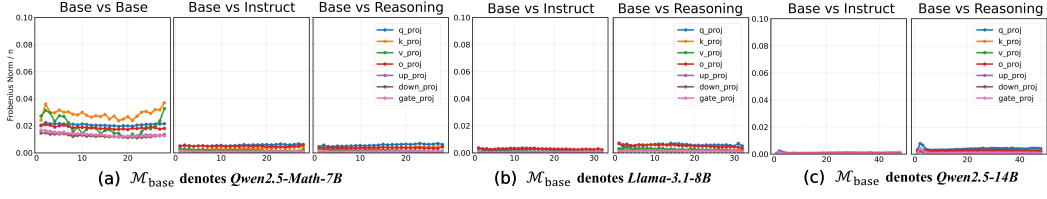


Figure 9: Extensively verifies the equality of $Q_1^{(i)}$ and $Q_2^{(i)}$ comparing $\mathcal{M}_{\text{base}}$ to $\mathcal{M}_{\text{post}}$ by $\mathcal{NF}^{(i)}$.

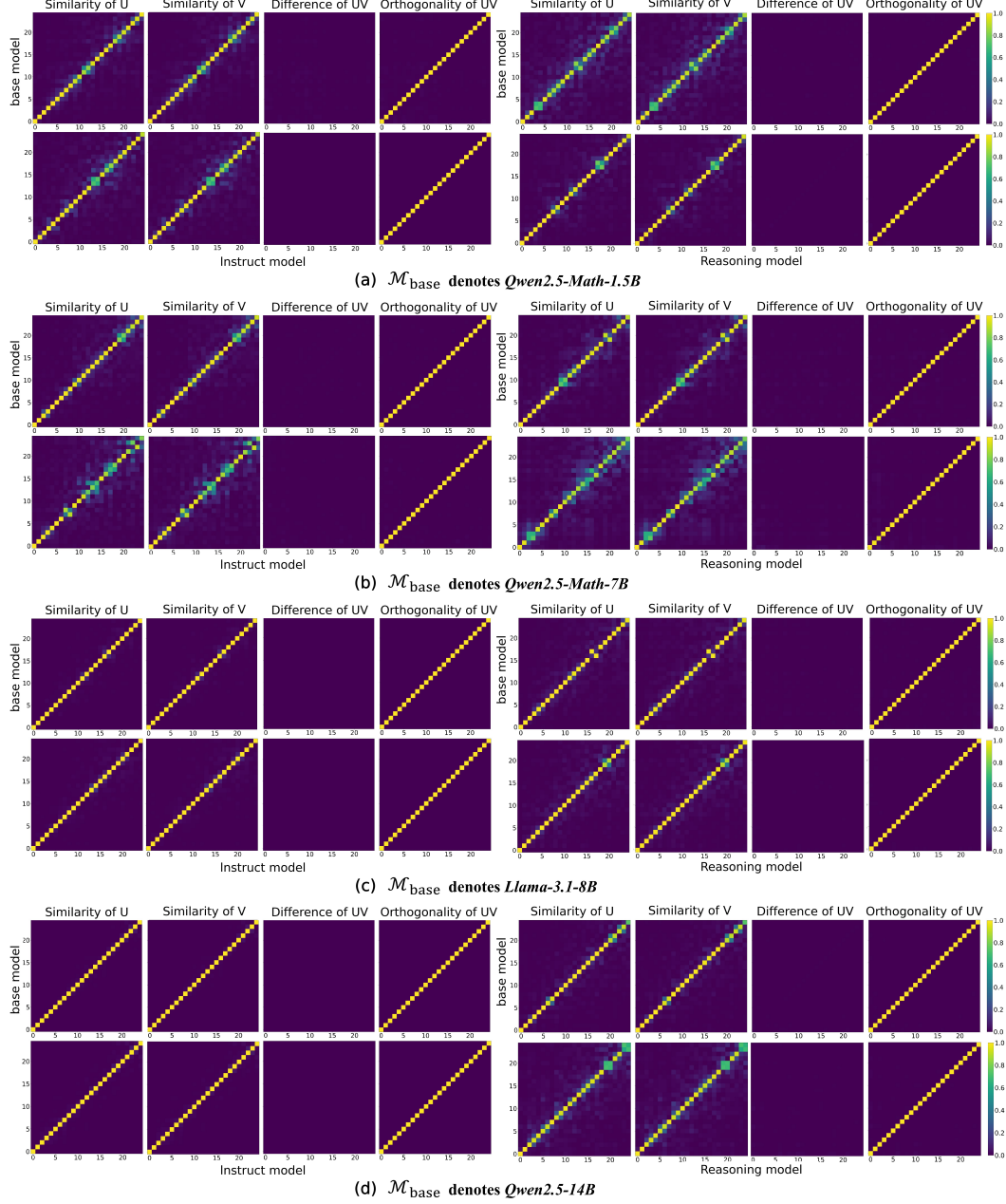


Figure 10: Visualizations of the similarity, difference and orthogonality matrices of the left and right singular vectors of the first and last Transformer block’s W_Q before and after post-training across models of different scales.

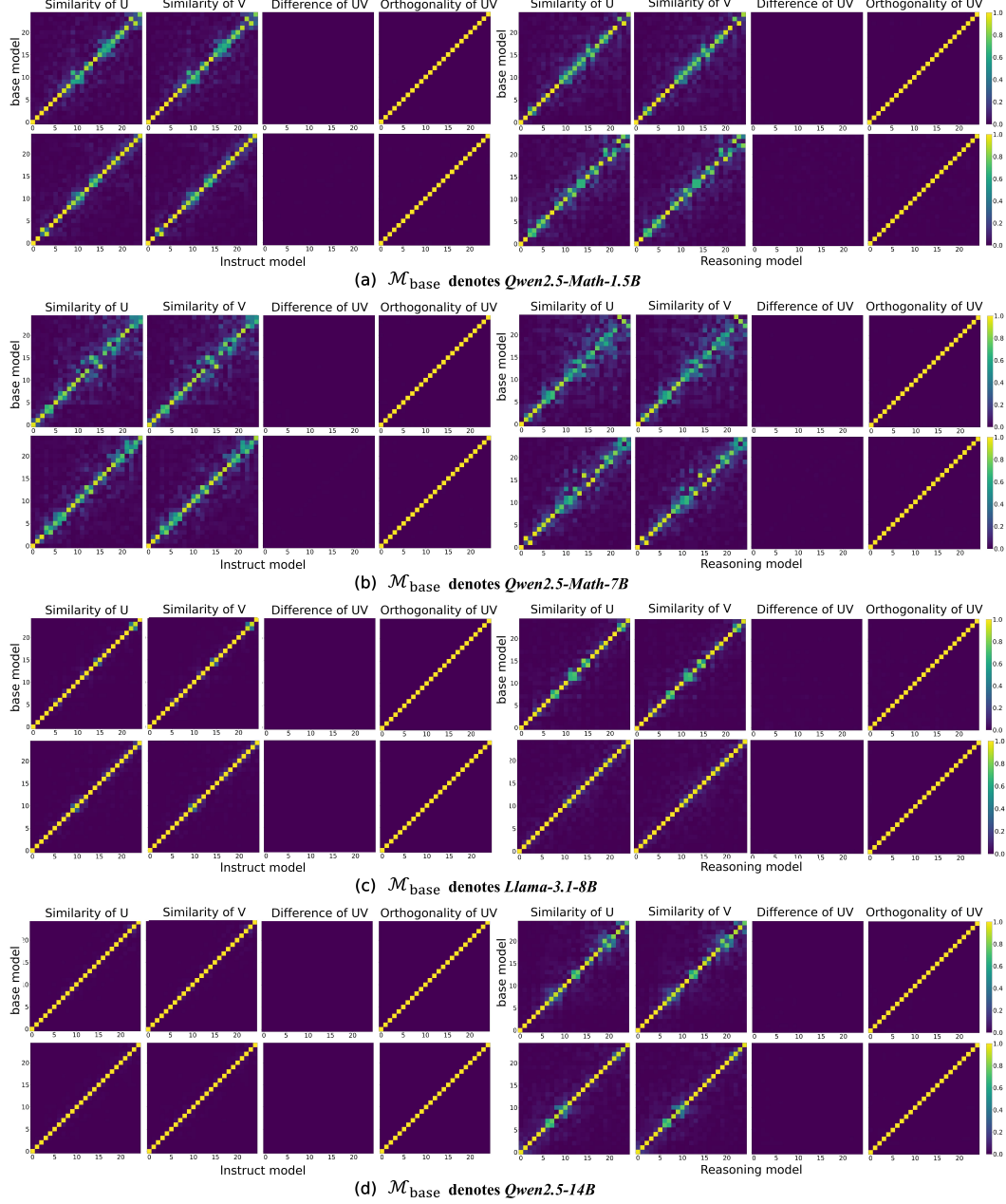


Figure 11: Visualizations of the similarity, difference and orthogonality matrices of the left and right singular vectors of the first and last Transformer block’s W_K before and after post-training across models of different scales.

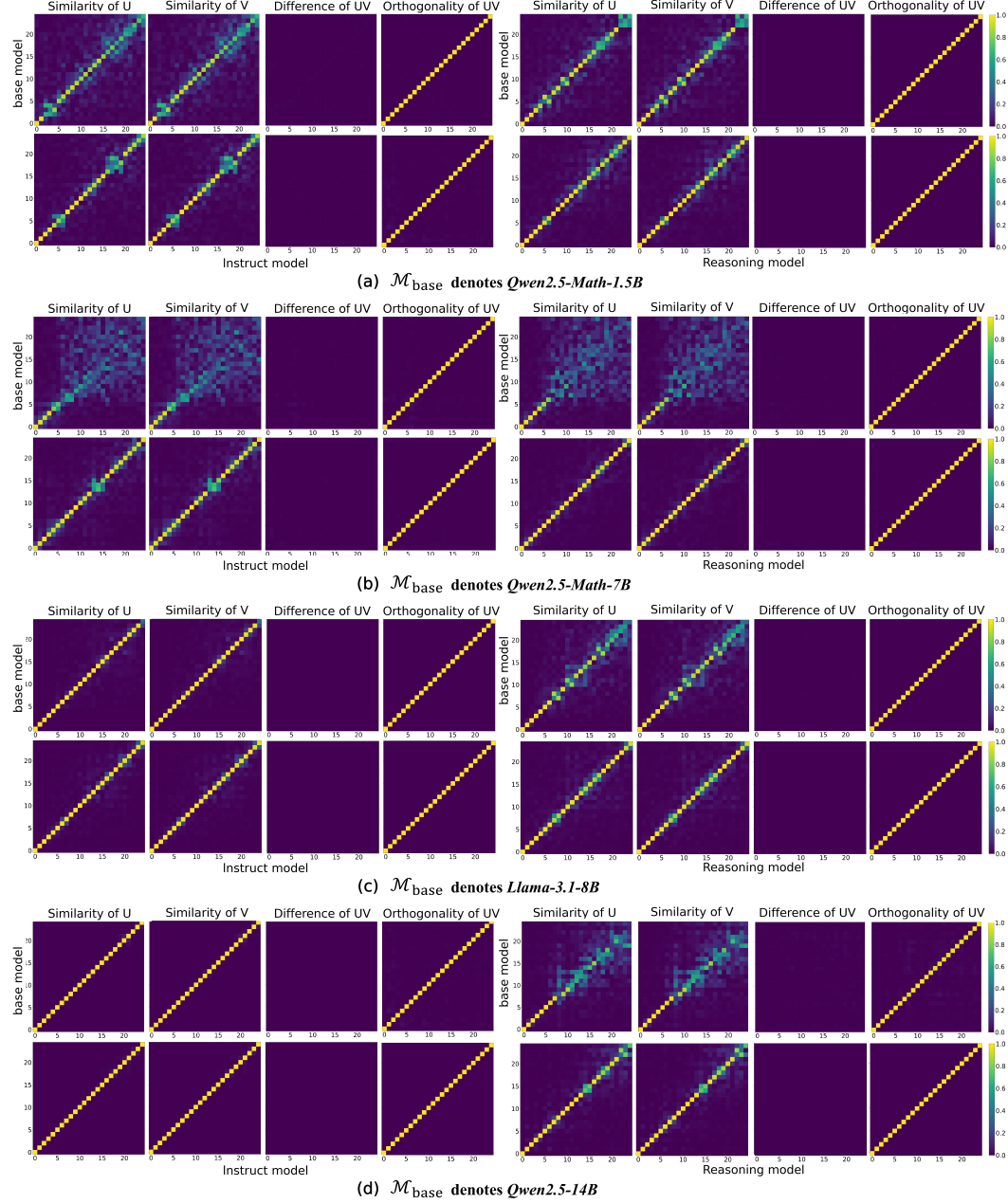


Figure 12: Visualizations of the similarity, difference and orthogonality matrices of the left and right singular vectors of the first and last Transformer block’s W_V before and after post-training across models of different scales.

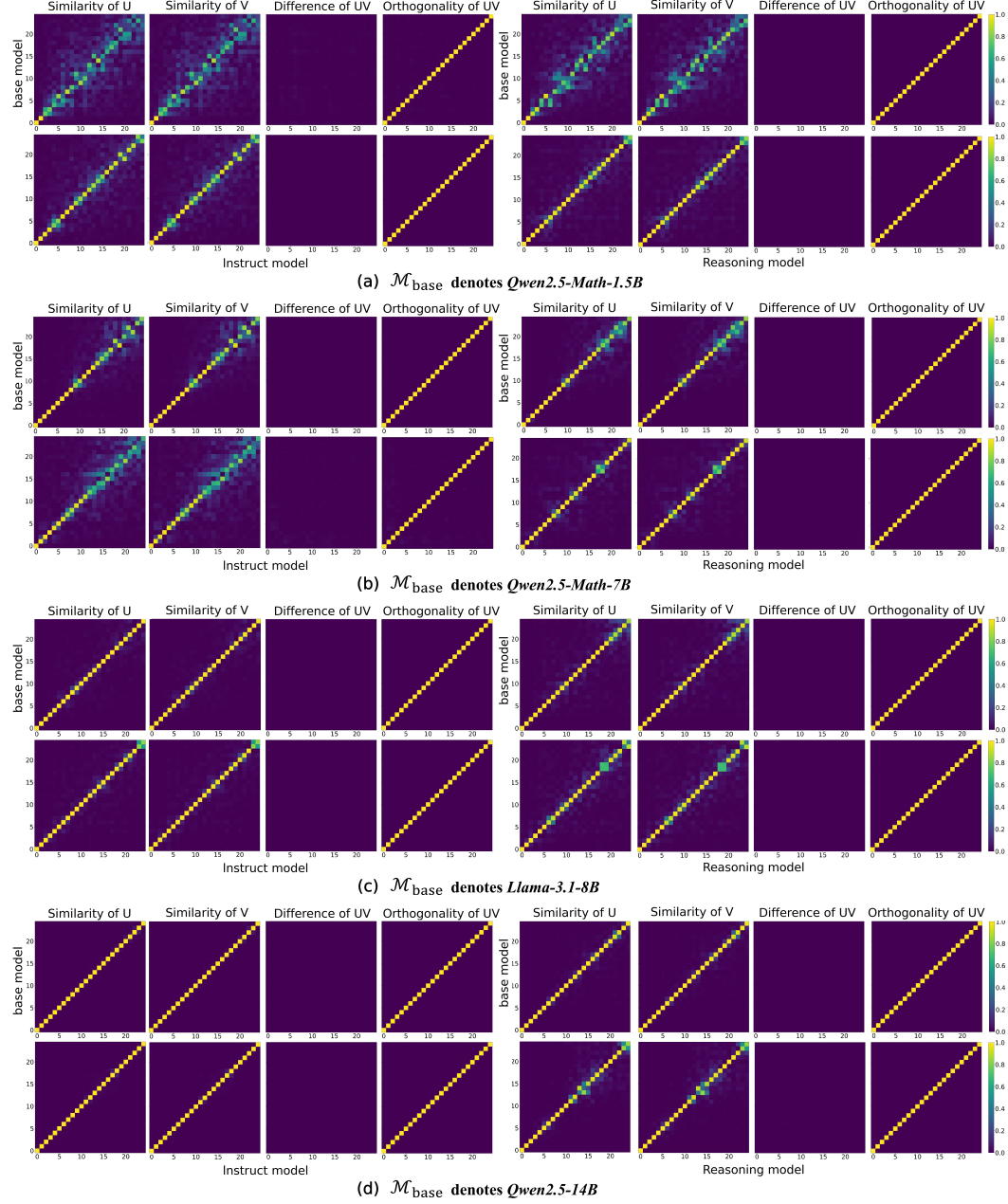


Figure 13: Visualizations of the similarity, difference and orthogonality matrices of the left and right singular vectors of the first and last Transformer block’s W_O before and after post-training across models of different scales.

We also observe that the similarity matrices of the left and right singular vectors are mostly concentrated along the diagonal. As shown in Appendix A, post-training does not alter the distribution of singular values of the weight matrices. When taken together with our current observation, this indirectly supports the view that post-training acts as a perturbation to the pretrained subspaces.

B.2 TRANSFORMATIONS OF SINGULAR VECTORS DURING PRE-TRAINING

The similarity matrices of the left and right singular vectors across different BASE models do not exhibit strong diagonal dominance, suggesting substantial divergence in their pretrained subspaces (Figure 14). Despite this divergence, we observe a subtle and consistent pattern in the orthogonal transformations between the left and right singular vectors. This subtle consistency may stem from an accumulation of alignment errors, implying that the orthogonal transformations are systematically misaligned to some extent. We can calibrate $U_{\text{post}}, V_{\text{post}}$ in Equation 8:

$$\begin{aligned} U_{\text{post}} &= U_{\text{base}}(Q \cdot \Delta Q_1) \\ V_{\text{post}} &= V_{\text{base}}(Q \cdot \Delta Q_2) \end{aligned} \quad (13)$$

The matrices ΔQ_1 and ΔQ_2 represent small-angle rotational components that capture fine-grained deviations superimposed on the coordinated rotation of the left and right singular vectors during training. These residual rotations correspond to the orthogonal perturbation term I_{orth} in Equation 7. From this perspective, the amount of data used in post-training is substantially smaller than in pre-training. As a result, the accumulated perturbations introduced during post-training are also much smaller than the large-scale rotations of the left and right singular vectors induced during pre-training. Given that the cumulative deviations introduced by ΔQ_1 and ΔQ_2 remain sufficiently small, the overall orthogonal transformations of the singular space can be well-approximated as coherent rotations. This also supports the validity of the approximation made in Equation 8.

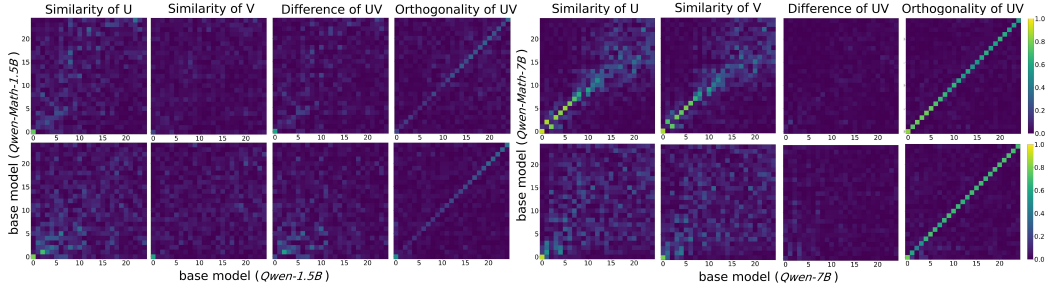


Figure 14: Visualizations of the similarity, difference and orthogonality matrices of the left and right singular vectors of the first and last Transformer block’s W_O between $\mathcal{M}_{\text{base}}$ and $\mathcal{M}'_{\text{base}}$.

C EXPERIMENTS ON DIFFERENT REPLACED MODELS

This section will conduct the same experiments as presented in the main paper on models of varying scales and families, aiming to verify the universality and generalizability of the near-uniform geometric scaling phenomenon of singular values. The evaluation will include tests on four standard benchmark datasets, along with visualizations of attention entropy.

C.1 PERFORMANCE OF DIFFERENT REPLACED MODELS

The purpose of performing Construction 9 on $\mathcal{M}_{\text{post}}$ is to verify that the singular value distribution of $\mathcal{M}_{\text{post}}$ can be reconstructed through the linear factor α' and the singular value distribution of $\mathcal{M}_{\text{base}}$, thereby validating the rationality of Equation 8. This verification critically depends on the selection of α' . Our choice of α' is based on Table 3, as it reflects the overall distribution of singular value scaling factors. We obtain the final α' values for each type of weight matrix in the post models by rounding the mean of these scaling factors, as presented in Table 4.

In our experiments, the output parameters of the LLMs are configured with a temperature of 0.2, a top_p of 0.95, and a maximum output token limit of 1024. This setting ensures stable generation while

Table 4: α' values (right) assigned based on mean singular value scaling factors (left) of weight matrices per type (from Table 3).

	POST Types	W_Q	W_K	W_V	W_O
<i>Qwen2.5-Math-1.5B</i>	$\mathcal{M}_{\text{Instruct}}$	0.9071 \rightarrow 0.9	0.9084 \rightarrow 0.9	0.9026 \rightarrow 0.9	0.9041 \rightarrow 0.9
	$\mathcal{M}_{\text{reasoning}}$	0.9710 \rightarrow 1.0	0.9723 \rightarrow 1.0	0.9513 \rightarrow 1.0	1.3551 \rightarrow 1.4
<i>Qwen2.5-Math-7B</i>	$\mathcal{M}_{\text{Instruct}}$	0.9074 \rightarrow 0.9	0.9103 \rightarrow 0.9	0.9040 \rightarrow 0.9	0.9056 \rightarrow 0.9
	$\mathcal{M}_{\text{reasoning}}$	0.9837 \rightarrow 1.0	0.9823 \rightarrow 1.0	0.9737 \rightarrow 1.0	1.3800 \rightarrow 1.4
<i>Llama-3.1-8B</i>	$\mathcal{M}_{\text{Instruct}}$	0.9960 \rightarrow 1.0	0.9951 \rightarrow 1.0	0.9957 \rightarrow 1.0	0.9975 \rightarrow 1.0
	$\mathcal{M}_{\text{reasoning}}$	1.0041 \rightarrow 1.0	0.9898 \rightarrow 1.0	0.9930 \rightarrow 1.0	1.4112 \rightarrow 1.4
<i>Qwen2.5-14B</i>	$\mathcal{M}_{\text{Instruct}}$	0.9990 \rightarrow 1.0	0.9989 \rightarrow 1.0	0.9989 \rightarrow 1.0	0.9989 \rightarrow 1.0
	$\mathcal{M}_{\text{reasoning}}$	0.9937 \rightarrow 1.0	0.9901 \rightarrow 1.0	0.9861 \rightarrow 1.0	1.3952 \rightarrow 1.4

	POST Types	W_{up}	W_{gate}	W_{down}
<i>Qwen2.5-Math-1.5B</i>	$\mathcal{M}_{\text{Instruct}}$	0.9016 \rightarrow 0.9	0.9018 \rightarrow 0.9	0.9019 \rightarrow 0.9
	$\mathcal{M}_{\text{reasoning}}$	0.9720 \rightarrow 1.0	0.9687 \rightarrow 1.0	0.9714 \rightarrow 1.0
<i>Qwen2.5-Math-7B</i>	$\mathcal{M}_{\text{Instruct}}$	0.9021 \rightarrow 0.9	0.9025 \rightarrow 0.9	0.9024 \rightarrow 0.9
	$\mathcal{M}_{\text{reasoning}}$	0.9847 \rightarrow 1.0	0.9839 \rightarrow 1.0	0.9843 \rightarrow 1.0
<i>Llama-3.1-8B</i>	$\mathcal{M}_{\text{Instruct}}$	0.9961 \rightarrow 1.0	0.9957 \rightarrow 1.0	0.9961 \rightarrow 1.0
	$\mathcal{M}_{\text{reasoning}}$	1.0036 \rightarrow 1.0	0.9988 \rightarrow 1.0	1.0035 \rightarrow 1.0
<i>Qwen2.5-14B</i>	$\mathcal{M}_{\text{Instruct}}$	0.9991 \rightarrow 1.0	0.9991 \rightarrow 1.0	0.9990 \rightarrow 1.0
	$\mathcal{M}_{\text{reasoning}}$	0.9922 \rightarrow 1.0	0.9924 \rightarrow 1.0	0.9909 \rightarrow 1.0

maintaining moderate diversity for subsequent statistical analysis. System prompts are provided in Appendix H.1. Each model is executed three times on the test set, with the final performance reported as the average score and variance. The results are presented in Table 5. The mean and variance of the average length of output tokens across three test runs are also reported in Table 6.

Table 5: Performance comparison between original and replaced models across GSM8K, MATH-500, MMLU, and GPQA with pass@1 accuracy(%).

BASE Models	REPLACED Types	GSM8K	MATH-500	MMLU (dev)	GPQA
<i>Qwen2.5-Math-7B</i>	$\mathcal{M}_{\text{Instruct}}$	95.75 \pm 0.12	70.06 \pm 0.50	55.90 \pm 0.16	27.14 \pm 0.49
	$\mathcal{M}_{\text{Instruct}}^{\text{replaced}}$	95.25\pm0.06	73.00\pm0.43	55.20\pm0.16	27.22\pm0.41
	$\mathcal{M}_{\text{reasoning}}$	62.70 \pm 1.05	47.60 \pm 0.33	58.71 \pm 0.91	14.73 \pm 0.97
	$\mathcal{M}_{\text{reasoning}}^{\text{replaced}}$	72.28\pm0.42	53.66\pm0.81	60.69\pm1.03	18.01\pm0.87
<i>Llama-3.1-8B</i>	$\mathcal{M}_{\text{Instruct}}$	34.70 \pm 1.24	31.46 \pm 1.06	67.48 \pm 0.44	21.21 \pm 0.29
	$\mathcal{M}_{\text{Instruct}}^{\text{replaced}}$	34.92\pm0.37	32.60\pm1.14	65.26\pm0.57	20.11\pm0.76
	$\mathcal{M}_{\text{reasoning}}$	60.17 \pm 0.07	32.73 \pm 0.41	52.51 \pm 1.47	11.40 \pm 0.17
	$\mathcal{M}_{\text{reasoning}}^{\text{replaced}}$	68.72\pm0.43	29.73\pm0.90	52.16\pm1.29	9.17\pm0.51
<i>Qwen2.5-14B</i>	$\mathcal{M}_{\text{Instruct}}$	94.24 \pm 0.29	70.53 \pm 0.34	90.63 \pm 0.16	36.65 \pm 0.36
	$\mathcal{M}_{\text{Instruct}}^{\text{replaced}}$	94.11\pm0.25	69.13\pm0.09	89.93\pm1.01	35.60\pm1.48
	$\mathcal{M}_{\text{reasoning}}$	70.61 \pm 0.46	53.13 \pm 0.25	77.89 \pm 0.76	19.48 \pm 0.55
	$\mathcal{M}_{\text{reasoning}}^{\text{replaced}}$	79.49\pm0.42	52.33\pm0.25	75.79\pm1.03	19.02\pm0.32

Experimental results demonstrate that models exhibit nearly identical performance before and after singular value replacement. This further validates that post-training does not alter the singular value distribution of pre-trained models, thereby supporting our conclusion.

Table 6: Comparison of average length of output tokens between Original and Replaced Models across GSM8K, MATH-500, MMLU, and GPQA.

BASE Models	REPLACED Types	GSM8K	MATH-500	MMLU (dev)	GPQA
<i>Qwen2.5-Math-1.5B</i>	$\mathcal{M}_{\text{Instruct}}$	305.01 \pm 1.54	542.32 \pm 1.21	402.60 \pm 3.13	633.82 \pm 5.09
	$\mathcal{M}_{\text{Instruct}}^{\text{replaced}}$	302.92\pm2.54	527.03\pm4.11	408.09\pm4.31	610.73\pm8.94
	$\mathcal{M}_{\text{reasoning}}$	539.82 \pm 6.86	911.55 \pm 5.55	619.34 \pm 13.82	952.00 \pm 18.83
	$\mathcal{M}_{\text{reasoning}}^{\text{replaced}}$	427.41\pm5.33	864.71\pm8.03	590.98\pm15.42	939.18\pm9.91
<i>Qwen2.5-Math-7B</i>	$\mathcal{M}_{\text{Instruct}}$	299.46 \pm 3.17	551.34 \pm 4.39	372.53 \pm 5.91	567.34 \pm 4.96
	$\mathcal{M}_{\text{Instruct}}^{\text{replaced}}$	304.21\pm2.91	549.13\pm2.53	378.34\pm4.51	533.19\pm5.98
	$\mathcal{M}_{\text{reasoning}}$	729.16 \pm 7.64	795.40 \pm 9.01	514.15 \pm 6.91	933.15 \pm 9.97
	$\mathcal{M}_{\text{reasoning}}^{\text{replaced}}$	451.27\pm9.28	726.08\pm6.14	488.30\pm15.17	891.63\pm6.07
<i>Llama-3.1-8B</i>	$\mathcal{M}_{\text{Instruct}}$	166.47 \pm 4.22	359.19 \pm 6.02	35.79 \pm 1.43	236.35 \pm 7.38
	$\mathcal{M}_{\text{Instruct}}^{\text{replaced}}$	146.05\pm2.18	451.38\pm7.71	41.42\pm3.36	251.64\pm3.06
	$\mathcal{M}_{\text{reasoning}}$	627.14 \pm 8.71	931.14 \pm 14.80	721.64 \pm 11.13	989.41 \pm 7.43
	$\mathcal{M}_{\text{reasoning}}^{\text{replaced}}$	651.23\pm11.34	970.02\pm15.14	751.02\pm8.29	994.00\pm4.31
<i>Qwen2.5-14B</i>	$\mathcal{M}_{\text{Instruct}}$	281.95 \pm 7.21	550.02 \pm 6.17	89.69 \pm 1.18	240.16 \pm 6.55
	$\mathcal{M}_{\text{Instruct}}^{\text{replaced}}$	299.14\pm5.11	530.65\pm5.93	87.56\pm2.43	241.67\pm6.39
	$\mathcal{M}_{\text{reasoning}}$	583.01 \pm 4.57	897.61 \pm 8.81	487.54 \pm 7.68	924.63 \pm 7.90
	$\mathcal{M}_{\text{reasoning}}^{\text{replaced}}$	410.97\pm7.81	847.14\pm2.06	514.09\pm6.90	933.15\pm5.10

We also observe that the performance of some REASONING models improves after singular value replacement. One possible explanation is that Construction 9 effectively eliminates noise arising from precision limitations or heterogeneous data during singular value adjustment of $\mathcal{M}_{\text{base}}$'s weight matrices in post-training phases. This reduction in noise consequently enables more efficient token consumption for simpler tasks (e.g., the notable decrease in output token count for $\mathcal{M}_{\text{reasoning}}^{\text{replaced}}$ of *Qwen2.5-Math-7B* on GSM8K). These observations suggest that post-training processes exert theoretically derivable influences on the singular values of weight matrices. We identify this phenomenon as a crucial direction for future theoretical investigation.

C.2 ATTENTION ENTROPY OF DIFFERENT REPLACED MODELS

To demonstrate that singular value scaling is similar to a temperature-controlled mechanism, we perform the following operation on all weight matrices W_{post} of the POST models:

$$W_{\text{post}} \leftarrow U_{\text{post}} \Sigma_{\text{base}} V_{\text{post}}^T \quad (14)$$

Construction 14 replaces the singular values of POST models' weight matrices with those from BASE models. To evaluate the impact of this substitution, we monitor the attention entropy \mathcal{H} . A substantial change in entropy suggests a shift in the distribution of attention scores, indicating a structural change. Otherwise, the effect may be interpreted as a soft temperature modulation.

We input example questions from different domains (Cobbe et al., 2021; Talmor et al., 2019; Hendrycks et al., 2021a; Rein et al., 2023) into replaced models $\mathcal{M}_{\text{replaced}}$ and observe their attention scores prior to generating the first token. Specifically, we track the average attention distribution from each attention head in Transformer blocks 0, 3, 5, 8, 10, 13, 15, 18, 20, 23, and 25, and compute the corresponding attention entropy.

QUESTION 1 (FROM GSM8K) :

Weng earns \$12 an hour for babysitting. Yesterday, she just did 50 minutes of babysitting. How much did she earn?

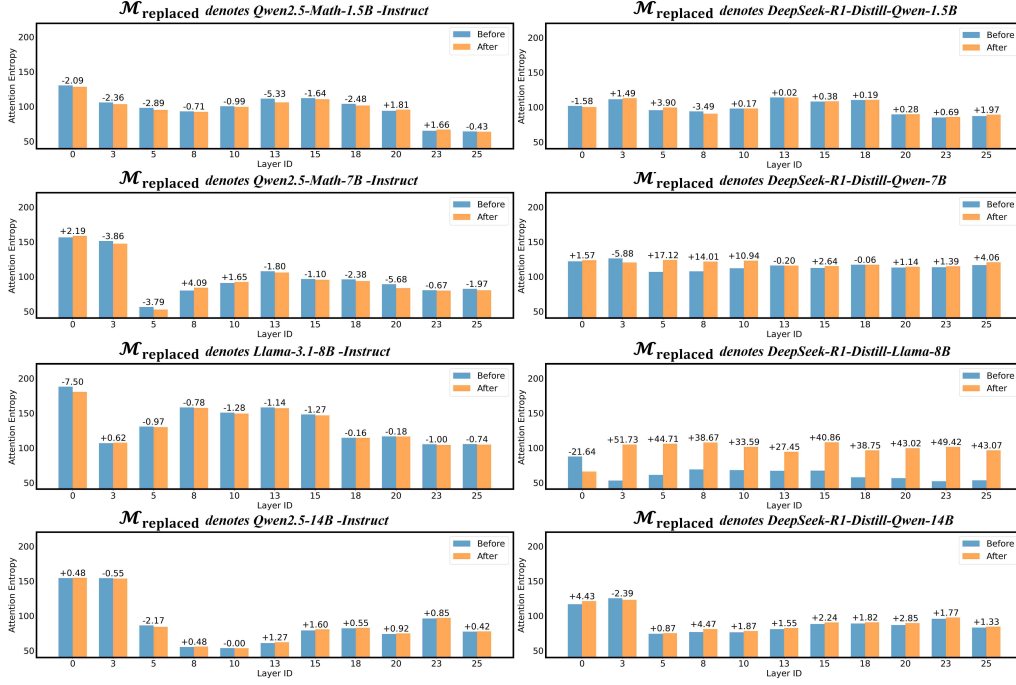


Figure 15: Attention entropy for different $\mathcal{M}_{\text{replaced}}$. The example input is from GSM8K.

QUESTION 2 (FROM MMLU_clinical_knowledge) :

What size of cannula would you use in a patient who needed a rapid blood transfusion (as of 2020 medical knowledge)?

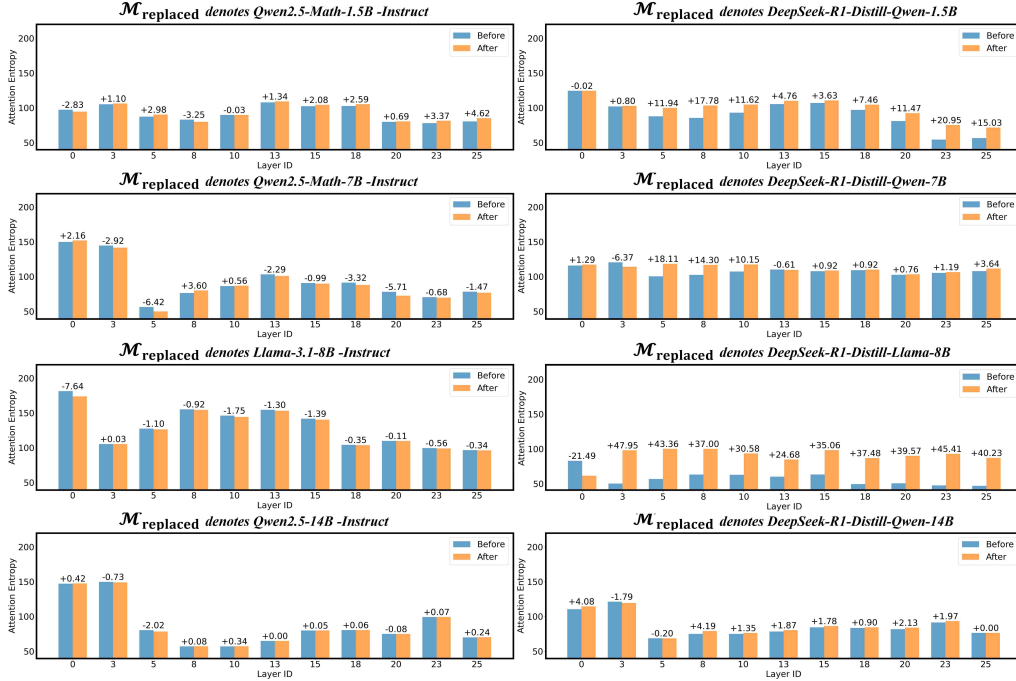
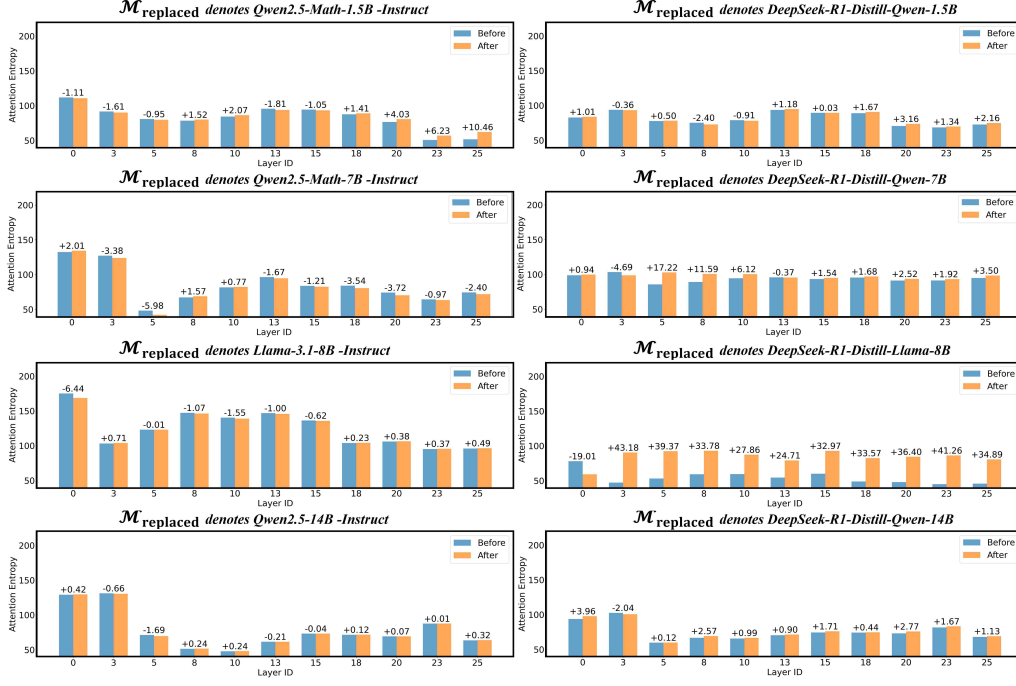


Figure 16: Attention entropy for different $\mathcal{M}_{\text{replaced}}$. The example input is from MMLU (clinical knowledge).

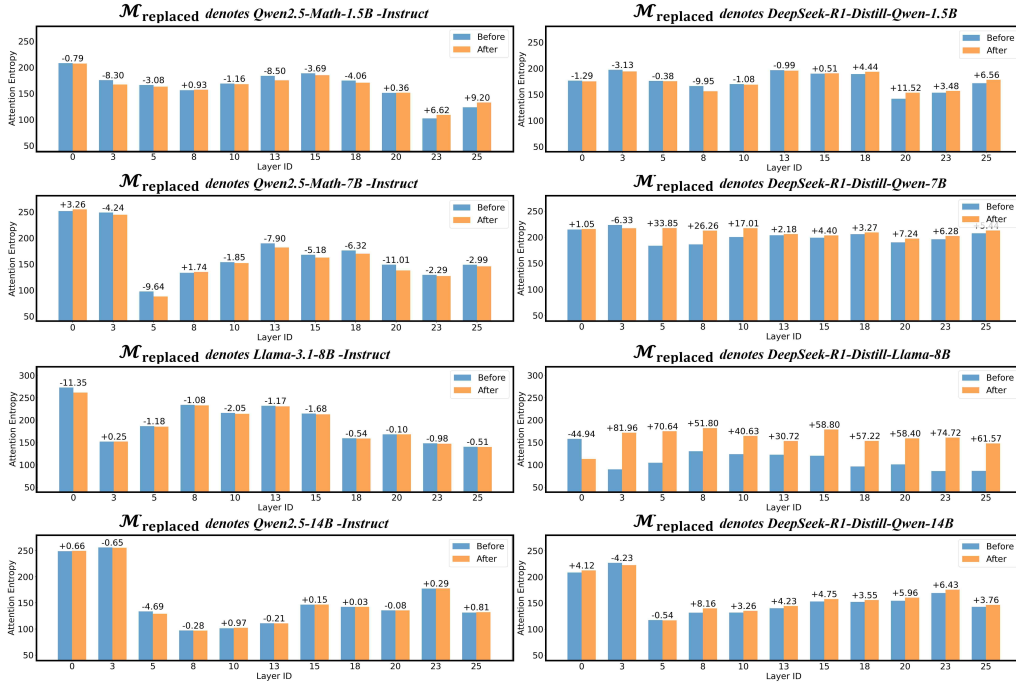
QUESTION 3 (FROM commonsenseQA) :

The sanctions against the school were a punishing blow, and they seemed to what the efforts the school had made to change?

Figure 17: Attention entropy for different $\mathcal{M}_{\text{replaced}}$. The example input is from CommonsenseQA.

QUESTION 4 (FROM GPQA_diamond) :

Two quantum states with energies E_1 and E_2 have a lifetime of 10^{-9} sec and 10^{-8} sec, respectively. We want to clearly distinguish these two energy levels. Which one of the following options could be their energy difference so that they be clearly resolved?

Figure 18: Attention entropy for different $\mathcal{M}_{\text{replaced}}$. The example input is from GPQA (diamond).

The replaced models $\mathcal{M}_{\text{replaced}}$, spanning diverse architectures and parameter scales, consistently preserve the attention entropy of their original counterparts across a range of examples. This robustness persists even under higher scaling of the singular values in the W_O of REASONING models. In particular, *Qwen*-based models exhibit minimal sensitivity to such modifications, with attention entropy remaining largely unchanged (Figures 15, 16, 17, 18). In contrast, *LLaMA*-based REASONING models show an increase in attention entropy when the overall scale of W_O singular values is reduced, consistent with a more uniform distribution of attention scores. Importantly, these effects are largely invariant to extreme amplification of singular values in the long tail of the spectrum, likely due to their negligible magnitude and limited contribution to the model’s functional behavior. These findings support the interpretation of global singular value scaling as a temperature-like mechanism for modulating attention sharpness.

D EXPERIMENTS ON VERIFYING THE CONSISTENCY OF ORTHOGONAL TRANSFORMATIONS

This section highlights the critical importance of orthogonal consistency. While the main paper only demonstrates that disrupting orthogonal transformations in SA output subspaces can be compensated by preserving orthogonality in input subspaces, we present here a more extensive set of experimental results. We apply Construction 10 to matrices in $\mathcal{M}_{\text{post}}$ to obtain $\mathcal{M}_{\text{post}}^{\text{ablation}}$, and use Construction 11 to derive $\mathcal{M}_{\text{post}}^{\text{restoration}}$. These operations model the destruction and subsequent restoration of the output subspaces in the weight matrices. Similarly, we apply Constructions 15 and 16 to the input subspaces, as a symmetric counterpart to Constructions 10 and 11:

$$W_{\text{post}}^{(i)} \leftarrow U_{\text{base}}^{(i)} \Sigma_{\text{post}} \cdot V_{\text{post}}^{(i)T} \quad (15)$$

$$W_{\text{post}}^{(i)} \leftarrow (U_{\text{base}}^{(i)} Q) \cdot \Sigma_{\text{post}} V_{\text{post}}^{(i)T} = (U_{\text{base}}^{(i)} \cdot V_{\text{base}}^{(i)T} V_{\text{post}}^{(i)}) \cdot \Sigma_{\text{post}} V_{\text{post}}^{(i)T} \quad (16)$$

Constructions 10, 11, 15, and 16 provide an intuitive demonstration of the orthogonal consistency between the left and right singular vectors of each weight matrix in the model. For each $\mathcal{M}_{\text{post}}$, we apply the transformations from Constructions 10, 11, 15, and 16 to all SA or FFN modules. These operations disrupt the orthogonal transformations of either the input or output subspaces, and attempt to restore them using the corresponding orthogonal mappings. This yields eight model variants: $\mathcal{M}_{\text{ablation}}^{SA, \text{out}}$, $\mathcal{M}_{\text{restoration}}^{SA, \text{out}}$, $\mathcal{M}_{\text{ablation}}^{SA, \text{in}}$, $\mathcal{M}_{\text{restoration}}^{SA, \text{in}}$, $\mathcal{M}_{\text{ablation}}^{FFN, \text{out}}$, $\mathcal{M}_{\text{restoration}}^{FFN, \text{out}}$, $\mathcal{M}_{\text{ablation}}^{FFN, \text{in}}$, and $\mathcal{M}_{\text{restoration}}^{FFN, \text{in}}$. The superscript indicates whether the operation is applied to the input or output subspaces of all weight matrices in SAs or FFNs, while the subscript denotes whether the operation is destructive or restorative. We perform ablation and restoration operations on SAs and FFNs separately, to prevent model collapse caused by excessive cumulative errors when restoring all weight matrices simultaneously. Additionally, this approach enables independent validation of the co-rotation phenomenon between the input-output subspaces of SAs and FFNs, avoiding excessive cumulative errors that could interfere with experimental observations.

D.1 PERFORMANCE OF DIFFERENT RESTORATION MODELS

We report the performance of all RESTORATION models on GSM8K, MATH-500, MMLU (dev split), and GPQA. All experimental configurations remain consistent with Appendix C.1, specifically with the temperature set to 0.2, top_p to 0.95, and a maximum output token length of 1024. The system prompts are as detailed in Appendix H.1. For each of the four datasets, we measure the results three times and report their pass@1 accuracy (%). All ABLATION models were unable to produce valid outputs, inevitably yielding a pass@1 accuracy of 0% in every evaluation. As these uniformly null results do not provide additional empirical insight, we refrain from reporting them in detail. The complete results are shown in Table 7 and 8.

Most RESTORATION models successfully recover the original performance, validating the consistency of co-rotational alignment between input and output subspaces and confirming Equation 8. We further observe that orthogonal substitutions in the output subspaces are more stable than in the input subspaces: $\mathcal{M}_{\text{restoration}}^{SA, \text{in}}$ often performs far worse than $\mathcal{M}_{\text{restoration}}^{SA, \text{out}}$, indicating directional rotational error (Appendix B.2). Errors appear to accumulate along the input-to-output pathway, while reverse elimination can cause collapse. This suggests an inherent asymmetry in co-rotation speed, with one subspace consistently leading the other—an intriguing phenomenon warranting further study.

Table 7: Performance comparison between original and RESTORATION models across GSM8K, MATH-500, MMLU, and GPQA with pass@1 accuracy(%). The "-" indicates model collapse.

BASE Models	POST Types	RESTORATION Types	GSM8K	MATH-500	MMLU (dev)	GPQA
<i>Qwen2.5-Math-1.5B</i>	$\mathcal{M}_{\text{Instruct}}$	$\mathcal{M}_{\text{original}}$	85.14 \pm 0.14	65.47 \pm 0.90	48.04 \pm 0.60	30.44 \pm 0.36
		$\mathcal{M}_{\text{restoration}}^{SA,in}$	84.53 \pm 0.25	66.20 \pm 0.16	41.28 \pm 0.44	27.69 \pm 0.29
		$\mathcal{M}_{\text{restoration}}^{SA,out}$	84.03 \pm 0.29	66.47 \pm 1.79	38.25 \pm 2.30	29.34 \pm 2.65
		$\mathcal{M}_{\text{restoration}}^{FFN,in}$	61.54 \pm 0.19	53.00 \pm 0.20	31.81 \pm 0.41	28.79 \pm 0.83
		$\mathcal{M}_{\text{restoration}}^{FFN,out}$	84.51 \pm 0.18	66.07 \pm 0.31	41.17 \pm 0.88	22.97 \pm 1.10
	$\mathcal{M}_{\text{Reasoning}}$	$\mathcal{M}_{\text{original}}$	62.88 \pm 0.59	32.73 \pm 1.64	25.02 \pm 0.59	7.02 \pm 0.44
		$\mathcal{M}_{\text{restoration}}^{SA,in}$	61.54 \pm 1.19	30.93 \pm 0.57	29.00 \pm 0.44	6.75 \pm 0.27
		$\mathcal{M}_{\text{restoration}}^{SA,out}$	61.96 \pm 1.71	32.06 \pm 0.25	28.30 \pm 1.77	3.45 \pm 1.23
		$\mathcal{M}_{\text{restoration}}^{FFN,in}$	60.60 \pm 1.25	53.60 \pm 0.43	25.49 \pm 1.07	12.81 \pm 1.44
		$\mathcal{M}_{\text{restoration}}^{FFN,out}$	76.05 \pm 0.71	56.46 \pm 0.34	32.51 \pm 3.03	16.71 \pm 1.81
<i>Qwen2.5-Math-7B</i>	$\mathcal{M}_{\text{Instruct}}$	$\mathcal{M}_{\text{original}}$	95.75 \pm 0.12	70.06 \pm 0.50	55.90 \pm 0.16	27.14 \pm 0.49
		$\mathcal{M}_{\text{restoration}}^{SA,in}$	95.15 \pm 0.41	73.20 \pm 0.33	55.18 \pm 0.18	24.85 \pm 0.17
		$\mathcal{M}_{\text{restoration}}^{SA,out}$	94.31 \pm 0.98	72.40 \pm 0.53	53.10 \pm 1.46	20.80 \pm 1.60
		$\mathcal{M}_{\text{restoration}}^{FFN,in}$	86.10 \pm 0.53	68.60 \pm 1.40	54.04 \pm 0.61	25.07 \pm 0.98
		$\mathcal{M}_{\text{restoration}}^{FFN,out}$	94.21 \pm 0.86	70.93 \pm 1.51	55.44 \pm 3.35	25.89 \pm 1.44
	$\mathcal{M}_{\text{Reasoning}}$	$\mathcal{M}_{\text{original}}$	62.70 \pm 1.05	47.60 \pm 0.33	58.71 \pm 0.91	14.73 \pm 0.97
		$\mathcal{M}_{\text{restoration}}^{SA,in}$	63.21 \pm 0.91	52.80 \pm 0.28	58.48 \pm 0.65	22.99 \pm 1.19
		$\mathcal{M}_{\text{restoration}}^{SA,out}$	64.34 \pm 2.29	50.93 \pm 1.36	59.06 \pm 0.73	21.34 \pm 0.69
		$\mathcal{M}_{\text{restoration}}^{FFN,in}$	82.46 \pm 0.90	65.60 \pm 2.91	48.42 \pm 0.70	22.71 \pm 1.13
		$\mathcal{M}_{\text{restoration}}^{FFN,out}$	58.83 \pm 1.66	60.07 \pm 1.75	58.83 \pm 0.73	20.16 \pm 2.42
<i>Llama-3.1-8B</i>	$\mathcal{M}_{\text{Instruct}}$	$\mathcal{M}_{\text{original}}$	34.70 \pm 1.24	31.46 \pm 1.06	67.48 \pm 0.44	21.21 \pm 0.29
		$\mathcal{M}_{\text{restoration}}^{SA,in}$	30.15 \pm 0.82	30.40 \pm 0.75	65.49 \pm 0.43	22.32 \pm 0.09
		$\mathcal{M}_{\text{restoration}}^{SA,out}$	31.18 \pm 1.17	33.13 \pm 1.70	63.74 \pm 2.66	25.07 \pm 2.16
		$\mathcal{M}_{\text{restoration}}^{FFN,in}$	24.13 \pm 2.12	23.40 \pm 1.91	59.64 \pm 0.93	22.61 \pm 1.19
		$\mathcal{M}_{\text{restoration}}^{FFN,out}$	43.97 \pm 2.06	23.26 \pm 1.28	63.62 \pm 2.92	21.98 \pm 1.29
	$\mathcal{M}_{\text{Reasoning}}$	$\mathcal{M}_{\text{original}}$	60.17 \pm 0.07	32.73 \pm 0.41	52.51 \pm 1.47	11.40 \pm 0.17
		$\mathcal{M}_{\text{restoration}}^{SA,in}$	60.30 \pm 1.54	29.60 \pm 0.49	42.22 \pm 0.59	8.77 \pm 0.60
		$\mathcal{M}_{\text{restoration}}^{SA,out}$	61.25 \pm 0.78	34.87 \pm 1.17	47.13 \pm 2.28	6.81 \pm 1.63
		$\mathcal{M}_{\text{restoration}}^{FFN,in}$	39.87 \pm 1.13	15.33 \pm 3.89	38.95 \pm 0.70	8.99 \pm 2.13
		$\mathcal{M}_{\text{restoration}}^{FFN,out}$	38.76 \pm 1.09	25.00 \pm 2.31	47.83 \pm 1.93	7.53 \pm 1.50
<i>Qwen2.5-14B</i>	$\mathcal{M}_{\text{Instruct}}$	$\mathcal{M}_{\text{original}}$	94.24 \pm 0.29	70.53 \pm 0.34	90.63 \pm 0.16	36.65 \pm 0.36
		$\mathcal{M}_{\text{restoration}}^{SA,in}$	94.09 \pm 0.34	68.86 \pm 0.50	88.42 \pm 0.29	37.60 \pm 0.34
		$\mathcal{M}_{\text{restoration}}^{SA,out}$	93.91 \pm 1.52	73.67 \pm 0.92	88.07 \pm 1.95	32.51 \pm 0.63
		$\mathcal{M}_{\text{restoration}}^{FFN,in}$	93.63 \pm 0.38	71.33 \pm 0.83	82.57 \pm 3.58	28.89 \pm 1.66
		$\mathcal{M}_{\text{restoration}}^{FFN,out}$	94.87 \pm 0.64	73.60 \pm 1.11	88.30 \pm 0.73	34.05 \pm 3.40
	$\mathcal{M}_{\text{Reasoning}}$	$\mathcal{M}_{\text{original}}$	70.61 \pm 0.46	53.13 \pm 0.25	77.89 \pm 0.76	19.48 \pm 0.55
		$\mathcal{M}_{\text{restoration}}^{SA,in}$	75.72 \pm 0.25	56.46 \pm 0.24	76.37 \pm 1.85	21.94 \pm 0.86
		$\mathcal{M}_{\text{restoration}}^{SA,out}$	76.32 \pm 1.69	56.33 \pm 1.70	78.83 \pm 3.06	17.17 \pm 1.91
		$\mathcal{M}_{\text{restoration}}^{FFN,in}$	-	-	-	-
		$\mathcal{M}_{\text{restoration}}^{FFN,out}$	82.15 \pm 1.41	62.60 \pm 1.39	76.84 \pm 3.35	27.06 \pm 3.95

Table 8: Comparison of average length of output tokens between original and RESTORATION Models across GSM8K, MATH-500, MMLU, and GPQA. The ”-” indicates model collapse.

BASE Models	POST Types	RESTORATION Types	GSM8K	MATH-500	MMLU (dev)	GPQA
<i>Qwen2.5-Math-1.5B</i>	$\mathcal{M}_{\text{Instruct}}$	$\mathcal{M}_{\text{original}}$	305.01 \pm 1.54	542.32 \pm 1.21	402.60 \pm 3.13	633.82 \pm 5.09
		$\mathcal{M}_{\text{restoration}}^{SA,in}$	309.47 \pm 15.81	523.06 \pm 5.87	435.36 \pm 8.72	646.07 \pm 6.98
		$\mathcal{M}_{\text{restoration}}^{SA,out}$	287.12 \pm 6.99	558.05 \pm 3.83	447.05 \pm 8.25	631.88 \pm 3.64
		$\mathcal{M}_{\text{restoration}}^{FFN,in}$	422.87 \pm 25.85	587.42 \pm 7.66	532.19 \pm 4.54	792.16 \pm 7.86
		$\mathcal{M}_{\text{restoration}}^{FFN,out}$	320.65 \pm 8.86	499.06 \pm 13.76	443.56 \pm 1.18	617.73 \pm 2.57
	$\mathcal{M}_{\text{Reasoning}}$	$\mathcal{M}_{\text{original}}$	539.82 \pm 6.86	911.55 \pm 5.55	619.34 \pm 13.82	952.00 \pm 18.83
		$\mathcal{M}_{\text{restoration}}^{SA,in}$	504.75 \pm 24.05	916.60 \pm 8.58	659.16 \pm 8.78	920.66 \pm 13.58
		$\mathcal{M}_{\text{restoration}}^{SA,out}$	518.82 \pm 10.24	910.68 \pm 19.32	661.64 \pm 13.52	968.31 \pm 4.19
		$\mathcal{M}_{\text{restoration}}^{FFN,in}$	356.13 \pm 11.35	692.21 \pm 6.48	466.14 \pm 10.31	872.22 \pm 16.03
		$\mathcal{M}_{\text{restoration}}^{FFN,out}$	422.74 \pm 4.12	755.90 \pm 5.98	502.26 \pm 8.86	819.93 \pm 4.54
<i>Qwen2.5-Math-7B</i>	$\mathcal{M}_{\text{Instruct}}$	$\mathcal{M}_{\text{original}}$	299.46 \pm 3.17	551.34 \pm 4.39	372.53 \pm 5.91	567.34 \pm 4.96
		$\mathcal{M}_{\text{restoration}}^{SA,in}$	320.01 \pm 9.72	561.23 \pm 4.63	411.70 \pm 3.47	665.44 \pm 10.30
		$\mathcal{M}_{\text{restoration}}^{SA,out}$	307.38 \pm 7.85	565.77 \pm 15.30	420.34 \pm 9.38	672.78 \pm 7.23
		$\mathcal{M}_{\text{restoration}}^{FFN,in}$	382.13 \pm 8.09	552.38 \pm 3.86	642.14 \pm 10.25	846.68 \pm 8.97
		$\mathcal{M}_{\text{restoration}}^{FFN,out}$	286.25 \pm 22.59	510.28 \pm 11.25	345.16 \pm 8.75	535.02 \pm 5.42
	$\mathcal{M}_{\text{Reasoning}}$	$\mathcal{M}_{\text{original}}$	729.16 \pm 7.64	795.40 \pm 9.01	514.15 \pm 6.91	933.15 \pm 9.97
		$\mathcal{M}_{\text{restoration}}^{SA,in}$	791.97 \pm 21.19	617.83 \pm 4.76	457.57 \pm 2.16	863.81 \pm 2.92
		$\mathcal{M}_{\text{restoration}}^{SA,out}$	796.48 \pm 5.62	778.33 \pm 5.57	451.87 \pm 7.65	877.55 \pm 17.99
		$\mathcal{M}_{\text{restoration}}^{FFN,in}$	423.84 \pm 8.60	809.49 \pm 8.49	388.25 \pm 7.09	824.16 \pm 3.86
		$\mathcal{M}_{\text{restoration}}^{FFN,out}$	442.44 \pm 14.48	691.19 \pm 7.95	444.99 \pm 12.73	823.32 \pm 13.92
<i>Llama-3.1-8B</i>	$\mathcal{M}_{\text{Instruct}}$	$\mathcal{M}_{\text{original}}$	166.47 \pm 4.22	359.19 \pm 6.02	35.79 \pm 1.43	236.35 \pm 7.38
		$\mathcal{M}_{\text{restoration}}^{SA,in}$	183.11 \pm 8.15	324.01 \pm 2.05	32.51 \pm 8.96	243.30 \pm 10.17
		$\mathcal{M}_{\text{restoration}}^{SA,out}$	169.65 \pm 4.65	343.88 \pm 18.92	48.50 \pm 6.12	254.77 \pm 9.58
		$\mathcal{M}_{\text{restoration}}^{FFN,in}$	150.22 \pm 3.90	278.5 \pm 11.29	5.33 \pm 1.24	6.01 \pm 1.42
		$\mathcal{M}_{\text{restoration}}^{FFN,out}$	173.32 \pm 7.98	247.75 \pm 13.73	11.01 \pm 1.41	38.74 \pm 1.11
	$\mathcal{M}_{\text{Reasoning}}$	$\mathcal{M}_{\text{original}}$	627.14 \pm 8.71	931.14 \pm 14.80	721.64 \pm 11.13	989.41 \pm 7.43
		$\mathcal{M}_{\text{restoration}}^{SA,in}$	410.23 \pm 6.32	833.03 \pm 11.39	755.99 \pm 15.07	989.68 \pm 3.84
		$\mathcal{M}_{\text{restoration}}^{SA,out}$	431.48 \pm 18.15	888.37 \pm 17.35	768.72 \pm 11.06	998.85 \pm 6.39
		$\mathcal{M}_{\text{restoration}}^{FFN,in}$	309.76 \pm 24.51	953.37 \pm 14.71	684.11 \pm 19.56	975.54 \pm 17.14
		$\mathcal{M}_{\text{restoration}}^{FFN,out}$	457.27 \pm 10.21	833.03 \pm 11.39	672.14 \pm 9.32	972.02 \pm 4.06
<i>Qwen2.5-14B</i>	$\mathcal{M}_{\text{Instruct}}$	$\mathcal{M}_{\text{original}}$	281.95 \pm 7.21	550.02 \pm 6.17	89.69 \pm 1.18	240.16 \pm 6.55
		$\mathcal{M}_{\text{restoration}}^{SA,in}$	279.14 \pm 7.21	444.63 \pm 13.24	101.63 \pm 8.73	283.74 \pm 9.02
		$\mathcal{M}_{\text{restoration}}^{SA,out}$	182.34 \pm 4.57	850.45 \pm 11.08	99.50 \pm 5.92	275.19 \pm 6.80
		$\mathcal{M}_{\text{restoration}}^{FFN,in}$	288.07 \pm 14.29	442.79 \pm 4.03	89.41 \pm 3.21	188.08 \pm 5.28
		$\mathcal{M}_{\text{restoration}}^{FFN,out}$	282.67 \pm 6.75	431.10 \pm 6.25	120.54 \pm 11.45	217.08 \pm 4.71
	$\mathcal{M}_{\text{Reasoning}}$	$\mathcal{M}_{\text{original}}$	583.01 \pm 4.57	897.61 \pm 8.81	487.54 \pm 7.68	924.63 \pm 7.90
		$\mathcal{M}_{\text{restoration}}^{SA,in}$	538.26 \pm 6.08	844.46 \pm 8.89	442.49 \pm 12.38	920.88 \pm 4.77
		$\mathcal{M}_{\text{restoration}}^{SA,out}$	518.71 \pm 11.25	852.79 \pm 9.55	438.20 \pm 4.33	912.47 \pm 5.40
		$\mathcal{M}_{\text{restoration}}^{FFN,in}$	-	-	-	-
		$\mathcal{M}_{\text{restoration}}^{FFN,out}$	504.96 \pm 8.01	863.77 \pm 3.59	450.66 \pm 10.42	875.01 \pm 11.63

D.2 CKA ANALYSIS OF DIFFERENT RESTORATION MODELS

We then feed N input examples into $\mathcal{M}_{\text{post}}$, $\mathcal{M}_{\text{post}}^{\text{ablation}}$, and $\mathcal{M}_{\text{post}}^{\text{restoration}}$, and compute the mean hidden representations $r_{\mathcal{M}}^{(i)}$ for each layer by averaging their outputs (Equation 17):

$$r_{\mathcal{M}}^{(i)} = \frac{1}{N} \sum_{j=1}^N \mathcal{M}^{(i)}(T_j) \quad (17)$$

where T_j is the j -th input question, and $\mathcal{M}^{(i)}(\cdot)$ denotes the hidden representation produced by the i -th Transformer block in model \mathcal{M} . We use the first 100 examples from the GSM8K training set for analysis ($N = 100$). We compute the CKA heatmap between the average hidden representations of $\mathcal{M}_{\text{post}}$ and each ABLATION/RESTORATION variant to assess the impact of orthogonal consistency on internal representations. Figure 19 presents our experimental results.

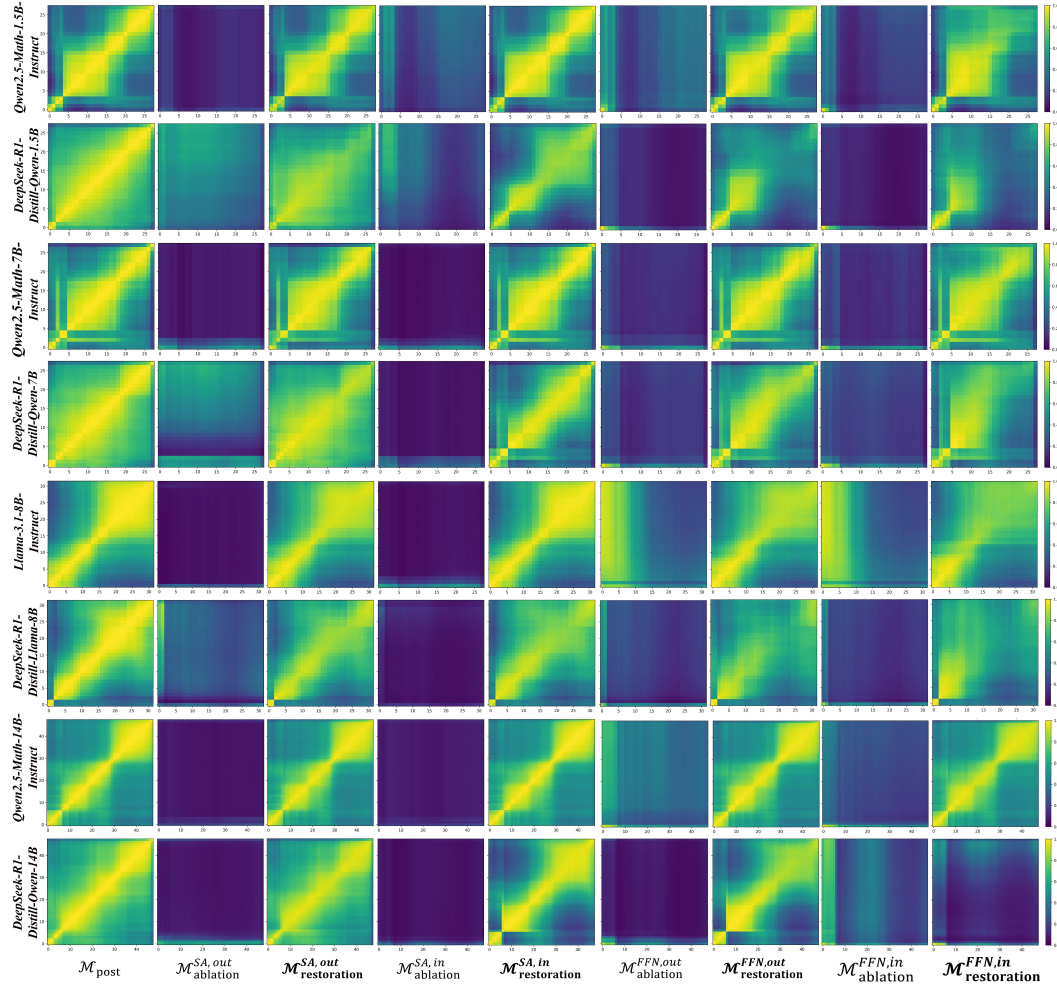


Figure 19: CKA heatmaps generated using $\mathcal{M}_{\text{post}}$ for $\mathcal{M}_{\text{post}}$, $\mathcal{M}_{\text{ablation}}$, and $\mathcal{M}_{\text{restoration}}$. The results indicate that $\mathcal{M}_{\text{Instruct}}$ exhibits stronger orthogonal alignment between input and output subspaces compared to $\mathcal{M}_{\text{reasoning}}$. Additionally, the restoration of orthogonal alignment after perturbation is more robust in the output subspaces than in the input subspaces.

Disrupting either the SAs or FFNs compromises the orthogonal alignment between input and output subspaces, impairing the internal structure of $\mathcal{M}_{\text{post}}$. Restoring this alignment leads to the reemergence of structural symmetry in the CKA heatmaps, indicating a partial recovery of the model’s

hidden representations. The weight matrices of $\mathcal{M}_{\text{Instruct}}$ exhibit stronger orthogonal consistency than those of $\mathcal{M}_{\text{reasoning}}$. This is evidenced by the restoration variants of $\mathcal{M}_{\text{Instruct}}$ producing CKA heatmaps that more closely resemble those of $\mathcal{M}_{\text{post}}$. The CKA heatmaps remain only partially reducible, reflecting the fact that orthogonality is preserved only approximately. This observation is further supported by the correction introduced in Equation 13. The restoration process effectively reinstates the original representational geometry, highlighting the critical structural role of orthogonal transformations.

E THE STRUCTURAL CHANGES IN A BROADER RANGE OF MODELS

In the main text, as well as in Appendix A, B, C and D, we present a systematic comparison of structural changes in model weights before and after supervised post-training, with a particular focus on the *Qwen* and *LLaMA* families. We also report detailed experimental results that confirm the validity of Equation 8. These findings naturally motivate several follow-up questions:

1. How do reinforcement learning (RL)-based post-training methods influence model weights? From the perspective of parameter space, in what ways do their effects differ from those of supervised post-training, and what implications can be drawn?
2. Would modifications to the model architecture or the adoption of different training strategies affect the generalizability of the observed structural changes?

This section addresses these questions by extending our analysis to a broader set of models. The subsequent case studies provide strong evidence that the validity of Equation 8 is preserved across diverse settings—including supervised post-training, RL-based post-training, and variations in model architecture or training methodology. The two structural changes identified in the main text thus appear to generalize robustly across these scenarios.

E.1 STRUCTURAL CHANGES IN LLMs INDUCED BY RL-BASED POST-TRAINING

We investigate several state-of-the-art large language models trained with advanced reinforcement learning algorithms, including *AceMath-RL-Nemotron-7B* (Liu et al., 2024), *deepseek-math-7b-rl* (Shao et al., 2024), and *Seed-X-PPO-7B* (Cheng et al., 2025). These models respectively adopt advanced reinforcement learning approaches such as GRPO (DeepSeek-AI et al., 2025) and PPO (Schulman et al., 2017), originate from different research groups, and are built upon diverse training corpora (see Table 10 for details). This diversity in both algorithmic choices and data sources provides inherent support for the generalizability of our subsequent experimental results. We compute the SVSMs between those models and their BASE versions, the $\mathcal{NF}^{(i)}$, as well as the orthogonality matrices of the singular vector (e.g., $I_{orth}^{(0)}$ in the first Transformer block), and present the corresponding visualizations in Figures 20, 21, and 22.

From the SVSM heatmaps and the lower values of $\mathcal{NF}^{(i)}$, we observe that models subjected to RL-based post-training exhibit even more consistent structural changes than those trained with SFT-based post-training. **This strongly suggests that SFT-based and RL-based post-training methods possess a high degree of parameter equivalence, meaning that the effects they impose on model parameters are essentially identical.** Building upon this conclusion, one may infer that RL-based post-training is effectively equivalent to supervised post-training, notwithstanding previous studies (Chu et al., 2025) that have highlighted the ostensibly superior generalization capacity of reinforcement learning algorithms. **We further conjecture that this generalization advantage does not arise from the intrinsic design of RL algorithms themselves, but rather from the diversity of training data generated through reinforcement learning.** For instance, GRPO encourages the model to produce more diverse responses, which are then incorporated into the training process as additional samples. This analysis further explains the effectiveness of Long-CoT distillation. Its training procedure is equivalent to that of RL-based methods, ensuring comparable effects on model parameters, while its training data are more extensive and diverse than those of instruction tuning, enabling smaller models to achieve reasoning capabilities similar to large-scale RL-based models.

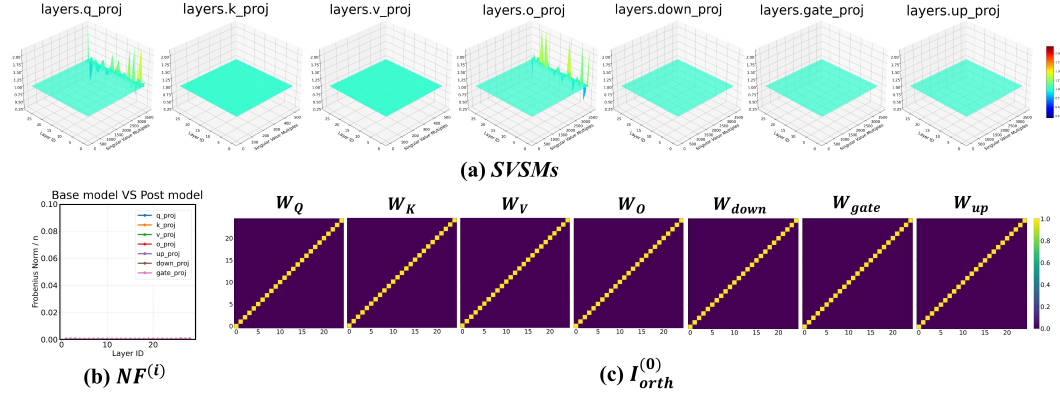


Figure 20: Visualization of structural properties of *AceMath-RL-Nemotron-7B* after post-training. (a) SVSMs reveal that the principal scaling exhibits a near-uniform distribution. (b) $N\mathcal{F}^{(i)}$ provides evidence for the consistent orthogonal transformations of the singular vectors. (c) Orthogonality matrices $I_{orth}^{(0)}$, shown as an example.

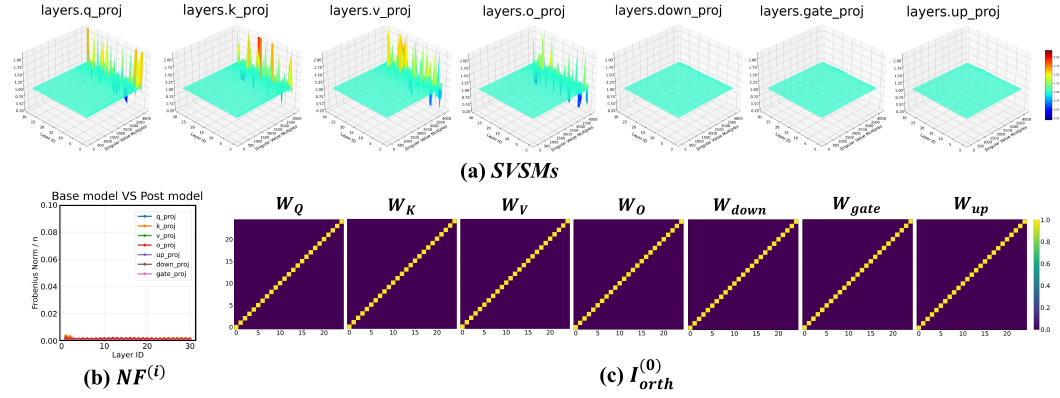


Figure 21: Visualization of structural properties of *deepseek-math-7b-rl* after post-training. The same set of analyses as in Figure 20 is presented, including SVSMs, $N\mathcal{F}^{(i)}$, and orthogonality matrices $I_{orth}^{(0)}$.

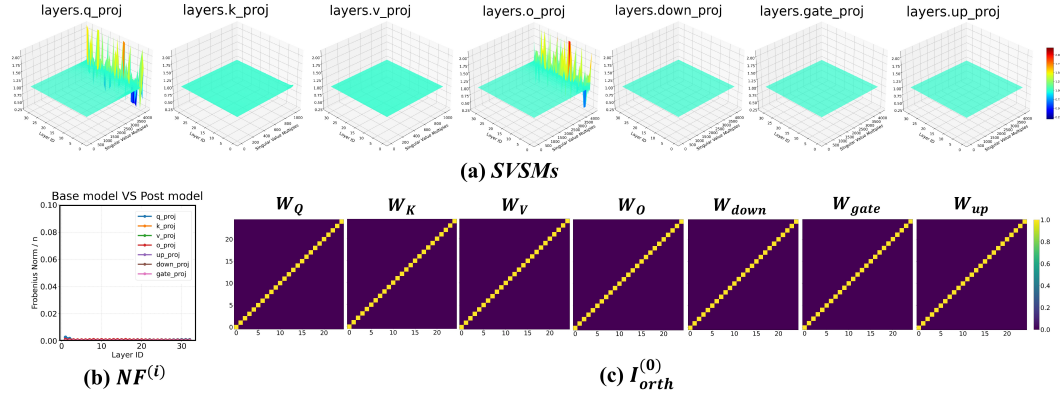


Figure 22: Visualization of structural properties of *Seed-X-PPO-7B* after post-training. The same set of analyses as in Figure 20 is presented, including SVSMs, $N\mathcal{F}^{(i)}$, and orthogonality matrices $I_{orth}^{(0)}$.

E.2 GENERALITY OF STRUCTURAL CHANGES ACROSS TRAINING STRATEGIES AND ARCHITECTURES

We find that **regardless of architectural modifications or training strategies, LLMs consistently exhibit these two structural changes in their parameters after post-training**. To further examine the universality of this phenomenon, we extend our analysis to *Mistral-7B-Instruct-v0.1* (Jiang et al., 2023), *Gemma-2-2B-it* (Gemma Team et al., 2024), and *MediPhi-Instruct* (Corbeil et al., 2025), each of which incorporates distinct design improvements:

- **For *Mistral-7B-Instruct-v0.1***, the model incorporates *Sliding Window Attention* (Beltagy et al., 2020) and a *Rolling Buffer Cache*. These mechanisms allow each layer’s hidden states to access past information within a window size W , which is recursively stacked across layers to effectively expand the attention span. As a result, the model achieves a theoretical attention span of approximately 131K tokens. In practice, these improvements substantially reduce memory consumption and enhance computational efficiency without compromising model quality.
- **For *Gemma-2-2B-it***, the model architecture integrates *local sliding window attention* (Beltagy et al., 2020) and *global attention* (Luong et al., 2015). Local layers operate with a window size of 4096 tokens, global layers extend to 8192 tokens. A *logit soft-capping* (Bello et al., 2017) mechanism stabilizes training across attention layers and the final layer, with soft_cap values set to 50.0 and 30.0. In post-training, the BASE model firstly undergoes supervised fine-tuning on a mixture of synthetic and human-generated English prompt–response pairs, and then proceeds to *Reinforcement learning with Human Feedback (RLHF)* (Ouyang et al., 2022), guided by a reward model trained on preference data to align behavior with human intent. The resulting models from each stage are averaged, improving stability and overall performance, and producing an instruction-tuned model optimized for both effectiveness and safety.
- **For *MediPhi-Instruct***, the model still follows a decoder-only Transformer architecture, but the computations of its SAs and FFNs differ from the previously mentioned models. In the case of SAs, given the input h , the query (Q), key (K), and value (V) are computed using a single weight matrix W_{QKV} :

$$Q, K, V = \text{chunk}(QKV), \quad QKV = hW_{QKV} \quad (18)$$

where $\text{chunk}(\cdot)$ splits QKV into Q, K, V along the last dimension. Similarly, for the FFNs, *MediPhi-Instruct* also merges W_{gate} and W_{up} . As a result, there are only four types of matrices in both the SAs and FFNs, namely W_{QKV} , W_O , $W_{\text{gate_up}}$ and W_{down} . In addition to the architectural modifications, *MediPhi-Instruct* also undergoes an SFT-based post-training stage that integrates domain-specific medical knowledge. Similar to other medical instruction-tuned models such as *Aloe* (Gururajan et al., 2024) and *Med42 v2* (Christophe et al., 2024), this stage leverages medical question-answering datasets and benchmark training sets such as *PubMedQA* (Jin et al., 2019), thereby aligning the model more closely with medical reasoning and instruction-following tasks.

More detailed information regarding the aforementioned models will be presented in Table 10. We compute the SVSMs between those models and their BASE versions, the $\mathcal{NF}^{(i)}$, as well as the orthogonality matrices of the singular vector (e.g., $I_{orth}^{(0)}$ in the first Transformer block), and present the corresponding visualizations in Figures 23, 24, and 25.

The flattened SVSM heatmaps and a relatively low value of $\mathcal{NF}^{(i)}$ indicate that, regardless of whether the modifications stem from changes in the model architecture or adjustments in the training strategy, this structural property consistently persists in the linear layers of large models. In other words, **Equation 8 can be employed to characterize the parameter changes of large models before and after post-training**. This provides strong evidence for the universality of such structural transformations and further substantiates the reliability of Equation 8.

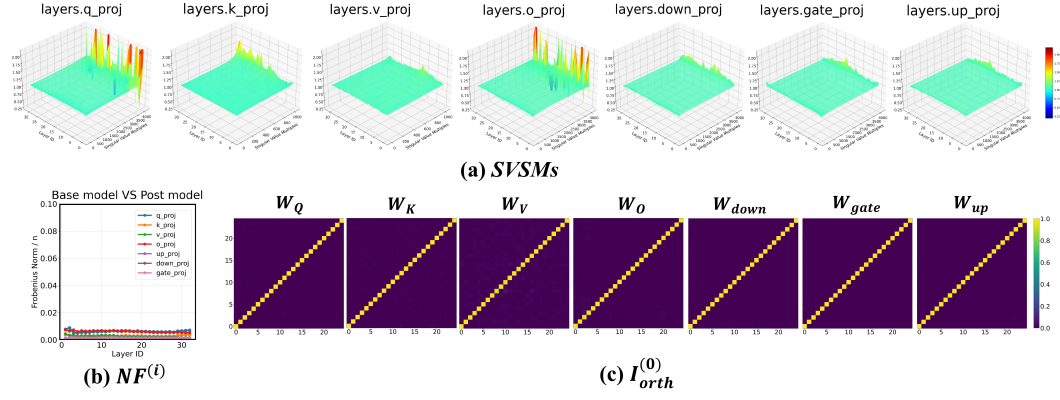


Figure 23: Visualization of structural properties of *Mistral-7B-Instruct-v0.1* after post-training. (a) SVSMs reveal that the principal scaling exhibits a near-uniform distribution. (b) $NF^{(i)}$ provides evidence for the consistent orthogonal transformations of the singular vectors. (c) Orthogonality matrices $I_{orth}^{(0)}$, shown as an example.

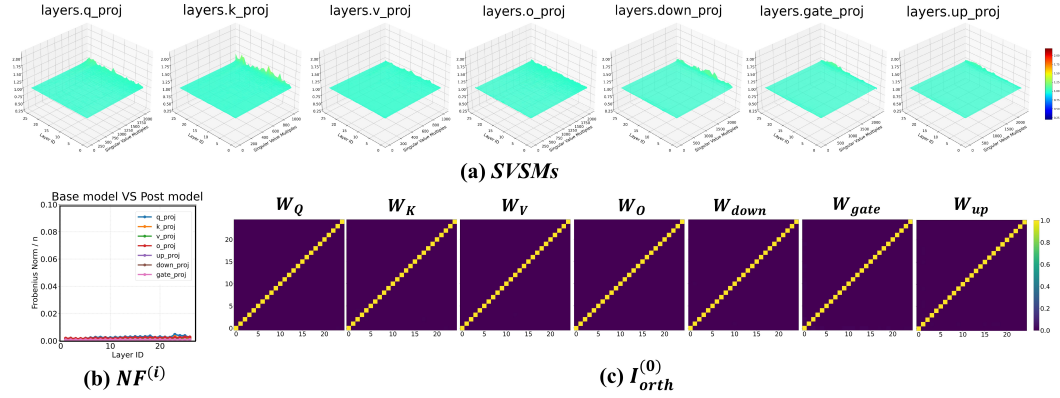


Figure 24: Visualization of structural properties of *Gemma-2-2B-it* after post-training. The same set of analyses as in Figure 23 is presented, including SVSMs, $NF^{(i)}$, and orthogonality matrices $I_{orth}^{(0)}$.

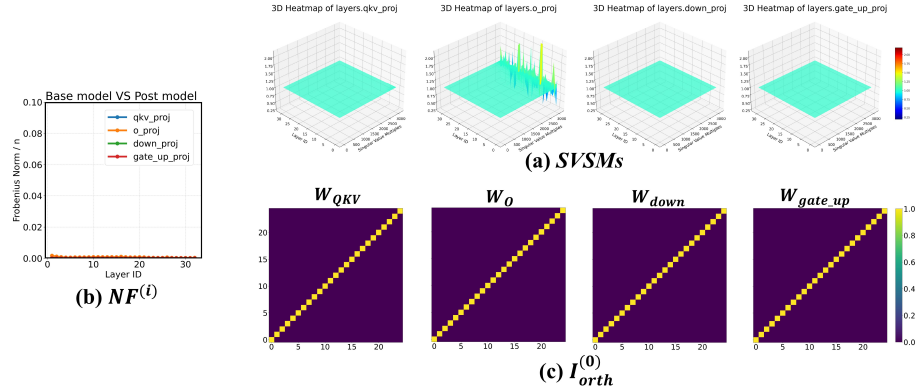


Figure 25: Visualization of structural properties of *MediPhi-Instruct* after post-training. The same set of analyses as in Figure 23 is presented, including SVSMs, $NF^{(i)}$, and orthogonality matrices $I_{orth}^{(0)}$.

F POTENTIAL APPLICATIONS OF OUR FINDINGS

While our primary focus is to characterize the structural transformations of LLMs induced by post-training, our analysis also points to several promising avenues for application. This section outlines a set of illustrative directions, intended not as definitive claims but as conceptual extensions of our findings, with the goal of inspiring future research and advancing the understanding of parameter-level transformations. An overview of these potential applications is provided in Figure 26.

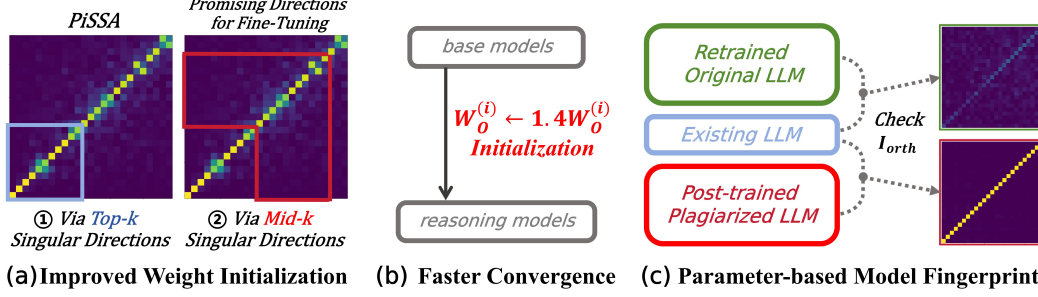


Figure 26: Illustrative overview of potential applications suggested by our findings: (a) fine-grained initialization strategies; (b) accelerated convergence in REASONING models; (c) model fingerprinting based on the detection of I_{orth} .

Fine-grained initialization strategies. From a post-training perspective, the observed coordinated rotation of singular vectors could inspire more fine-grained weight initialization strategies. A novel approach, termed *PiSSA* (Meng et al., 2024), preserves key components of singular vectors and singular values by initializing them as LoRA weights, while retaining and freezing the remaining singular components. However, *PiSSA* primarily fine-tunes the principal components corresponding to the top- k singular directions. Our analysis of sim_U and sim_V (Figures 10–13) reveals that the singular vectors associated with the largest singular values (σ_{max}) exhibit minimal rotation during post-training. This observation implies that the dominant singular components are not the primary targets of fine-tuning. Consequently, as shown in Figure 26a, directing fine-tuning toward the middle- k components rather than the top- k may yield improved performance.

Potentially accelerated convergence in REASONING models. We find that the singular value dynamics of REASONING models exhibits unique scaling patterns, particularly in matrices such as W_O (as demonstrated in Figures 2 and 7). Motivated by this observation, one may hypothesize that simple rescaling of pretrained singular values could accelerate convergence during reasoning-oriented training. For instance, initializing W_O as αW_O with $\alpha = 1.4$ provides a lightweight mechanism to impose reasoning-like spectral properties in a single step, potentially reducing the number of iterations required to reach stable performance. While speculative, this perspective highlights the potential to exploit post-training geometry for more efficient model development.

Model fingerprints under fully parameterized testing. Appendix B.2 demonstrates that the weight matrices of the same model architecture exhibit markedly different behaviors in I_{orth} after undergoing distinct pre-training and post-training procedures. This observation provides a practical criterion for distinguishing whether a large language model has been fully developed from scratch or merely obtained through post-training on another model. As illustrated in Figure 26c, this distinction can be achieved simply by measuring the deviation between I_{orth} and the identity matrix I . Importantly, since disrupting the coordinated rotational structure directly leads to model collapse, potential plagiarists cannot eliminate the discrepancy between their model and the original one by deliberately altering this property. Consequently, I_{orth} serves as a robust and discriminative fingerprint for model identification. Moreover, because this method relies solely on parameter-level analysis, it does not require the design of evaluation datasets as in representation-based fingerprinting approaches such as *REEF* (Zhang et al., 2024a). This line of investigation highlights a promising avenue for safeguarding the intellectual property rights of LLM developers.

While the potential applications discussed above represent relatively straightforward extensions of our observations, their concrete implementation and validation require more rigorous empirical investigation. Nevertheless, we hope that these preliminary intuitions will serve to inspire future

research and provide readers with a deeper understanding of the broader implications of our findings for model design, optimization, and interpretability.

G PROOF

This section mainly integrates all the mathematical proofs mentioned in the main paper.

G.1 SINGULAR VALUE SCALING MODULATES THE ATTENTION SCORE

Under near-uniform geometric scaling with singular values, Equation 8 can be restated as $W_{\text{post}} \approx \alpha \cdot U_{\text{post}} \Sigma_{\text{base}} V_{\text{post}}^T = \alpha \cdot W'_{\text{post}}$, which means scaling the singular values has the same effect as scaling the entire weight matrix. We uniformly apply this linear scaling effect to all weight matrices in SAs and FFNs, resulting in the following modified forms of Equations 1 and 2:

$$SA(h) \approx \text{softmax} \left(\frac{\alpha^2 \cdot hW'_Q \cdot [K'_{\text{cache}}; hW'_K]^T}{\sqrt{d}} \right) \cdot [V'_{\text{cache}}; hW'_V] \cdot W'_O \cdot \alpha \alpha_O \quad (19)$$

$$FFN(z) \approx (SwiGLU(z \cdot W'_{\text{gate}} \cdot \alpha) \odot (z \cdot W'_{\text{up}})) \cdot W'_{\text{down}} \cdot \alpha^2 \quad (20)$$

The term α^2 in Equation 19 corresponds to the inverse of the *attention temperature* (Vaswani et al., 2023), **which can be directly expressed by $T = 1/\alpha^2$** . In SAs, all α except α_O of REASONING models are consistently below 1 after post-training (demonstrated in Table 3), which corresponds to a higher attention temperature. This causes the softmax function to produce more uniformly distributed attention scores, encouraging the model to attend more evenly across all tokens and thereby enhancing its ability to capture global contextual information.

G.2 TRAINING IS TO PERFORM ORTHOGONAL TRANSFORMATION ON U AND V MATRICES

Considering $\mathcal{M}_A \rightarrow \mathcal{M}_B$ as the model training process, the left and right singular vectors of $W_A \in \mathcal{M}_A$ can be regarded as performing different transformations Q_U, Q_V :

$$U_B = U_A Q_U, \quad V_B = V_A Q_V \quad (21)$$

We prove that Q_U and Q_V must be orthogonal matrices. For Q_U, Q_V , we have:

$$\begin{aligned} U_A^T U_B &= U_A^T U_A \cdot Q_U = I \cdot Q_U = Q_U \\ V_A^T V_B &= V_A^T V_A \cdot Q_V = I \cdot Q_V = Q_V \end{aligned} \quad (22)$$

$Q^T Q = I$ is a necessary and sufficient condition for Q to be an orthogonal matrix. We calculate $Q_U^T Q_U$ and $Q_V^T Q_V$ then have:

$$\begin{aligned} Q_U^T Q_U &= (U_A^T U_B)^T \cdot (U_A^T U_B) = U_B^T \cdot (U_A U_A^T) \cdot U_B = I \\ Q_V^T Q_V &= (V_A^T V_B)^T \cdot (V_A^T V_B) = V_B^T \cdot (V_A V_A^T) \cdot V_B = I \end{aligned} \quad (23)$$

Therefore Q_U and Q_V are orthogonal matrices.

G.3 PROOF OF DIFFERENTLY POST-TRAINED MODELS SHARING A SET OF CONSISTENT ORTHOGONAL TRANSFORMATIONS

We theoretically prove that different POST models initialized from the same pretrained parameters and post-trained on data from different distributions can be transformed into each other through a set of shared orthogonal transformations. Assuming there are two POST models $\mathcal{M}_{\text{post}}, \mathcal{M}'_{\text{post}}$, combining equations 6 and 8, we have:

$$U_{\text{post}} = U_{\text{base}} Q_{\text{post}}, \quad V_{\text{post}} = V_{\text{base}} Q_{\text{post}} \quad (24)$$

$$U'_{\text{post}} = U_{\text{base}} Q'_{\text{post}}, \quad V'_{\text{post}} = V_{\text{base}} Q'_{\text{post}} \quad (25)$$

Substituting Equation 24 into 25, we have:

$$\begin{aligned} U'_{\text{post}} &= (U_{\text{post}} Q_{\text{post}}^T) \cdot Q'_{\text{post}} = U_{\text{post}} \cdot (Q_{\text{post}}^T Q'_{\text{post}}) \\ V'_{\text{post}} &= (V_{\text{post}} Q_{\text{post}}^T) \cdot Q'_{\text{post}} = V_{\text{post}} \cdot (Q_{\text{post}}^T Q'_{\text{post}}) \end{aligned} \quad (26)$$

Let $Q_{\text{combined}} = Q_{\text{post}}^T Q'_{\text{post}}$, then we observe that:

$$Q_{\text{combined}}^T Q_{\text{combined}} = (Q_{\text{post}}^T Q'_{\text{post}})^T (Q_{\text{post}}^T Q'_{\text{post}}) = I \quad (27)$$

Q_{combined} is an orthogonal matrix. This directly shows that the conversion from $\mathcal{M}_{\text{post}} \rightarrow \mathcal{M}'_{\text{post}}$ can be transformed using an approximately consistent orthogonal matrix Q_{combined} .

This significant corollary reveal that both in-distribution fine-tuning (e.g., instruction tuning) and out-of-distribution fine-tuning (e.g., Long-CoT distillation) induce equivalent transformations in parameter space—specifically, different post-training methods can be mutually converted through shared orthogonal transformations. This equivalence explains why LLMs can be fine-tuned on arbitrary data distributions to improve task-specific performance: **the model’s input and output subspaces undergo orthogonal transformations optimized for the target task distribution.** However, this also exposes a fundamental mechanism behind *catastrophic forgetting*: **when shared orthogonal transformations are disrupted and overwritten by new task-specific ones, the original transformations are lost, leading to performance degradation on prior tasks.**

We believe this insight offers significant promise for future research, particularly in developing methods to mitigate forgetting while preserving adaptability.

H SETTINGS

This section will delve into more detailed experimental setups, including the different system prompts used for various datasets and the precision of models.

H.1 SYSTEM PROMPTS

The datasets used in this study include GSM8K, MATH-500, MMLU, and GPQA. Due to time and cost constraints, we limit the output tokens to 1024. If a simple system prompt is used directly, models (particularly REASONING models) often require more tokens to generate correct answers when handling challenging datasets like GPQA. This would result in truncated outputs due to the token limit, preventing us from obtaining valid results for performance evaluation. Therefore, we need to design distinct system prompts for different datasets to facilitate observation of the outcomes.

Additionally, since some datasets provide descriptive ground-truth answers (e.g., GSM8K and MATH-500) while others present multiple-choice questions (e.g., MMLU and GPQA), we must also process the inputs differently across datasets to ensure accurate performance validation.

For the simple dataset (GSM8K) mentioned in this article, the unified system prompt we adopted is:

Please put your final answer within \boxed{\}.

Additionally, all visualization results, including the tracking of attention entropy and the analysis of CKA heatmaps, also adopt this simple system prompt. This is attributed to the fact that during visual analysis of the model, comprehensive output results or testing performance metrics are not required for evaluation purposes.

For hard datasets (MATH-500, MMLU and GPQA) mentioned in this article, the unified system prompt we adopted is:

Please put your final answer within \boxed{\} and keep your thought process as short as possible.

This system prompt will enable us to effectively measure the performance on hard datasets of models within limited token computations.

For the multiple-choice question datasets (MMLU and GPQA) mentioned in this text, the template we adopted for all input prompts is as follows:

{ORIGINAL QUESTION}
 You have four options, and they are:
 A. **{CHOICE A}**
 B. **{CHOICE B}**
 C. **{CHOICE C}**
 D. **{CHOICE D}**
 Please select the correct option and just give A, B, C or D. For example, if you think the answer is A, just give `\boxed{A}` as the answer.

This template design enables us to use the same validation evaluator for both multiple-choice and open-ended answer datasets, thereby reducing our engineering complexity.

H.2 INTRODUCTION TO THE MODELS AND MODEL PRECISION SETTINGS

The different POST versions corresponding to the different BASE models are shown in Table 9 and 10. All experiments in this paper were conducted on two NVIDIA A100 GPUs with 40GB of memory each.

Table 9: Different POST versions of different BASE models used in Appendix A, B, C and D.

BASE Models	POST Types	POST Models	Developer
<i>Qwen2.5-Math-1.5B</i>	$\mathcal{M}_{\text{Instruct}}$	<i>Qwen2.5-Math-1.5B-Instruct</i>	<i>Qwen Team</i>
	$\mathcal{M}_{\text{reasoning}}$	<i>DeepSeek-R1-Distill-Qwen-1.5B</i>	<i>DeepSeek</i>
<i>Qwen2.5-Math-7B</i>	$\mathcal{M}_{\text{Instruct}}$	<i>Qwen2.5-Math-7B-Instruct</i>	<i>Qwen Team</i>
	$\mathcal{M}_{\text{reasoning}}$	<i>DeepSeek-R1-Distill-Qwen-7B</i>	<i>DeepSeek</i>
<i>Llama-3.1-8B</i>	$\mathcal{M}_{\text{Instruct}}$	<i>Llama-3.1-8B-Instruct</i>	<i>Meta</i>
	$\mathcal{M}_{\text{reasoning}}$	<i>DeepSeek-R1-Distill-Llama-8B</i>	<i>DeepSeek</i>
<i>Qwen2.5-14B</i>	$\mathcal{M}_{\text{Instruct}}$	<i>Qwen2.5-14B-Instruct</i>	<i>Qwen Team</i>
	$\mathcal{M}_{\text{reasoning}}$	<i>DeepSeek-R1-Distill-Qwen-14B</i>	<i>DeepSeek</i>

Table 10: Different POST versions of different BASE models used in Appendix E.

BASE Models	POST Models	post-training method	Developer
<i>DeepSeek-R1-Distill-Qwen-7B</i>	<i>AceMath-RL-Nemotron-7B</i>	RL-based (GRPO)	<i>Nvidia</i>
<i>deepseek-math-7b-base</i>	<i>deepseek-math-7b-rl</i>	RL-based (GRPO)	<i>Deepseek</i>
<i>Seed-X-Instruct-7B</i>	<i>Seed-X-PPO-7B</i>	RL-based (PPO)	<i>ByteDance</i>
<i>Mistral-7B-v0.1</i>	<i>Mistral-7B-Instruct-v0.1</i>	SFT-based	<i>Mistral AI</i>
<i>gemma-2-2b</i>	<i>gemma-2-2b-it</i>	SFT-based	<i>Google</i>
<i>MediPhi</i>	<i>MediPhi-Instruct</i>	SFT-based	<i>Microsoft</i>

All $\mathcal{M}_{\text{base}}$ and $\mathcal{M}_{\text{Instruct}}$ use BF16 parameter storage, while $\mathcal{M}_{\text{reasoning}}$ employ FP32. To address potential precision truncation, we consistently convert all parameters to FP32 before experimentation, ensuring unified numerical precision throughout our evaluations.

I USE OF LARGE LANGUAGE MODELS

We acknowledge the use of LLMs for minor editorial assistance. Specifically, **LLMs were only employed to polish the language and correct grammatical errors in the manuscript**. No LLMs were involved in generating the research ideas, designing experiments, conducting analyses, or drawing conclusions.